


Spontaneous slow wave oscillations in extracellular field potential recordings reflect the alternating dominance of excitation and inhibition

Ying Zheng^{1,2} , Sungmin Kang³, Joseph O'Neill³ and Ingo Bojak^{2,4}

¹School of Biological Sciences, Whiteknights, University of Reading, Reading, UK

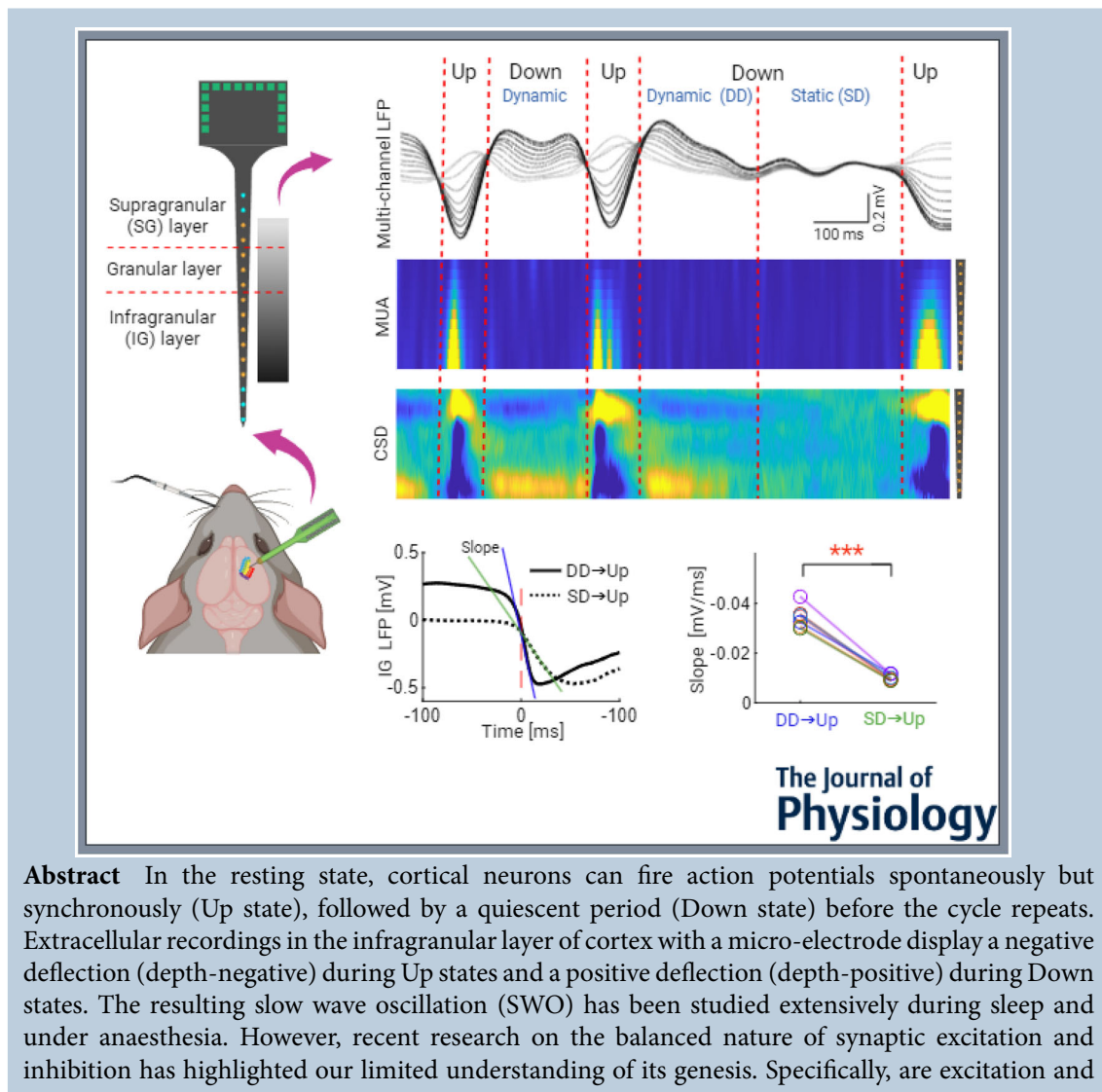
²Centre for Integrative Neuroscience and Neurodynamics (CINN), University of Reading, Reading, UK

³School of Psychology, Cardiff University, Cardiff, UK

⁴School of Psychology and Clinical Language Science, Whiteknights, University of Reading, Reading, UK

Handling Editors: David J. A. Wyllie & Gareth Morris

The peer review history is available in the Supporting Information section of this article (<https://doi.org/10.1113/JP284587#support-information-section>).



Abstract In the resting state, cortical neurons can fire action potentials spontaneously but synchronously (Up state), followed by a quiescent period (Down state) before the cycle repeats. Extracellular recordings in the infragranular layer of cortex with a micro-electrode display a negative deflection (depth-negative) during Up states and a positive deflection (depth-positive) during Down states. The resulting slow wave oscillation (SWO) has been studied extensively during sleep and under anaesthesia. However, recent research on the balanced nature of synaptic excitation and inhibition has highlighted our limited understanding of its genesis. Specifically, are excitation and

inhibition balanced during SWOs? We analyse spontaneous local field potentials (LFPs) during SWOs recorded from anaesthetised rats via a multi-channel laminar micro-electrode and show that the Down state consists of two distinct synaptic states: a Dynamic Down state associated with depth-positive LFPs and a prominent dipole in the extracellular field, and a Static Down state with negligible (≈ 0 mV) LFPs and a lack of dipoles extracellularly. We demonstrate that depth-negative and -positive LFPs are generated by a shift in the balance of synaptic excitation and inhibition from excitation dominance (depth-negative) to inhibition dominance (depth-positive) in the infragranular layer neurons. Thus, although excitation and inhibition co-tune overall, differences in their timing lead to an alternation of dominance, manifesting as SWOs. We further show that Up state initiation is significantly faster if the preceding Down state is dynamic rather than static. Our findings provide a coherent picture of the dependence of SWOs on synaptic activity.

(Received 23 February 2023; accepted after revision 15 January 2024; first published online 31 January 2024)

Corresponding author Y. Zheng: School of Biological Sciences, Whiteknights, University of Reading, Reading RG6 7AY, UK. Email: ying.zheng@reading.ac.uk

Abstract figure legend Local field potential (LFP) recordings during slow wave oscillation can be classified into three states: Up, Dynamic Down (DD), and Static Down (SD). These states have different signatures in the multichannel LFP time series and the corresponding current source density (CSD) maps, but multi-unit activity (MUA) maps cannot distinguish between the DD and SD states. Making the distinction revealed faster slopes of the LFP when transitioning from DD to Up as compared with SD to Up.

Key points

- Cortical neurons can exhibit repeated cycles of spontaneous activity interleaved with periods of relative silence, a phenomenon known as ‘slow wave oscillation’ (SWO).
- During SWOs, recordings of local field potentials (LFPs) in the neocortex show depth-negative deflection during the active period (Up state) and depth-positive deflection during the silent period (Down state).
- Here we further classified the Down state into a dynamic phase and a static phase based on a novel method of classification and revealed non-random, stereotypical sequences of the three states occurring with significantly different transitional kinetics.
- Our results suggest that the positive and negative deflections in the LFP reflect the shift of the instantaneous balance between excitatory and inhibitory synaptic activity of the local cortical neurons.
- The differences in transitional kinetics may imply distinct synaptic mechanisms for Up state initiation.
- The study may provide a new approach for investigating spontaneous brain rhythms.

Introduction

The term ‘slow wave oscillation’ (SWO) describes the observation of cortical and subcortical neural signals

that alternate spontaneously between periods associated with intense activity and relative quiescence, referred to as the Up and the Down states, respectively (Contreras & Steriade, 1995; Destexhe et al., 2007; Steriade et al.,

Ying Zheng is a professor in Systems Engineering and Neuroscience. Her current research focuses on understanding the relationship between extracellular field potential recordings and the underlying neuronal mechanisms.



1993; Timofeev et al., 2000). The phenomenon has been reported in humans and animals during sleep, as well as under certain levels of anaesthesia. It persists both *in vivo* and *in vitro*. Intracellularly, SWO is reflected in the membrane potential of a cortical neuron alternating between depolarisation (Up) and hyperpolarisation (Down). Extracellular markers of SWO include multi-unit activity (MUA) switching between active (Up) and baseline (Down) states, and local field potentials (LFPs) or the electroencephalogram (EEG) displaying depth-negative (Up) and depth-positive (Down) characteristics (Contreras et al., 1996; Haider & McCormick, 2009; Timofeev et al., 1996).

Mechanisms underlying the genesis of the Up and Down states have been studied by many researchers (for reviews, see for example McCormick et al., 2015; Neske, 2016; Timofeev et al., 2020). Both synaptic and intrinsic properties of cortical neurons are implicated (Compte et al., 2003a; McCormick & Pape, 1990; McCormick et al., 2003; Sanchez-Vives & McCormick, 2000; Schwindt et al., 1992; Steriade et al., 1993). Recent investigations have demonstrated that during SWO, and other brain rhythms such as gamma oscillations, the excitatory and inhibitory synaptic activities of cortical neurons co-vary and oscillate in similar patterns. Specifically, using whole cell patch clamp recording techniques during the Up state and transition to the Down state, excitatory and inhibitory synaptic conductances of cortical neurons were shown to both increase initially and subsequently decrease gradually, with the onset of inhibition lagging excitation by a few milliseconds and the instantaneous ratio of the two conductances varying during the active period (Atallah & Scanziani, 2009; Berg & Ditlevsen, 2013; Berg et al., 2007; Haider et al., 2006; Neske et al., 2015; Petersen et al., 2014; Rudolph et al., 2007; Shu et al., 2003).

There seems to be a straightforward interpretation of the Up and Down states in terms of membrane potential depolarisation and hyperpolarisation, or in terms of active and absent MUA. However, it is less clear how to interpret the depth-negative and depth-positive LFP characteristics, given that membrane potentials during Up and Down states are roughly maintained at their respective constant levels. Our current understanding is that the depth-negative LFP arises during the Up state because of recurrent network activity targeting neurons in layer V of the cortex, resulting in a net influx of excitatory post-synaptic current in the infragranular (IG) layer of the cortex and a net positive return current in the supragranular (SG) layer (Chauvette et al., 2010; Sanchez-Vives & McCormick, 2000). As for the depth-positive LFP observed during the Down state, one possible explanation is that the excitatory post-synaptic current may have reversed its direction of flow because dendritic compartments of neurons might

be more depolarised than the soma during the Down state (Chauvette et al., 2010). Another suggestion is that since the Down state is a non-synaptic event, the positive field potential in the IG layer might be the result of synchronised hyperpolarisation of local pyramidal neurons (Buzsáki et al., 2012). However, it is unclear what this purported hyperpolarising process entails.

Depth-positive LFP is not the only LFP marker associated with the Down state during SWOs. We often observe LFPs staying approximately at 0 mV in our data, particularly during prolonged Down states. Similar characteristics can be observed in LFP data from other studies (Saleem et al., 2010; Torao-Angosto et al., 2021). In this paper, we question the current interpretation of the depth-positive characteristics of the LFP and re-examine its neuronal mechanisms based not only on our own LFP data, but also on published data from whole cell patch-clamp recordings. The fundamental questions we seek answers to are the following:

- (i) The transition of membrane potentials from the Up to the Down state takes place typically within 100 ms (Chauvette et al., 2010; Neske et al., 2015; Sanchez-Vives et al., 2010; Timofeev et al., 2012) but the depth-positive LFP usually lasts much longer. What underlies this 'difference'?
- (ii) Is the depth-positive/surface-negative LFP during the Down state driven by the dominance of IPSCs in the soma compartment, or the dominance of EPSCs in the dendritic compartment, of IG layer pyramidal neurons?

We first examine the spontaneous Up and Down states present in the LFP data recorded in the barrel cortex of rats during SWOs induced by isoflurane anaesthesia and make a novel experimental distinction between a Dynamic Down (DD) and a Static Down (SD) state. The order of occurrence of these two different Down states is shown to be highly systematic. We then combine our results with research findings across the field to propose specific answers to the mentioned LFP phenomena.

Methods

Ethical approval

All experiments were carried out in accordance with the British Home Office regulations (Animals (Scientific Procedures) Act 1986) and approved by the Research Ethics Committee at the University of Reading, UK. Experimental procedures conformed to the principles and regulations of *The Journal of Physiology* (Grundy, 2015).

Animals

All experiments were performed on female Lister Hooded rats ($n = 7$) purchased from Charles River, Margate, Kent, UK. The body weight at the time of purchase ranged between 200 and 224 g. Rats were housed in a temperature (21°C) and humidity ($50 \pm 10\%$) controlled room with a 12-h dark–light cycle and *ad libitum* access to food and water. They were caged in groups of two to four and fed a standard chow diet (RM3 (E) 801 066, Special Diets Services, Witham, Essex, UK).

Surgery and manipulation of anaesthetic levels

On the day of surgery, rats weighing between 210 and 250 g were anaesthetised in an induction chamber supplied with 5% isoflurane (ISO) before moving to a stereotaxic holder. During surgery, ISO was supplied through a nose cone at 3% with an oxygen flow rate of 0.5 l/min. A thermostatic heating pad was inserted underneath the rat to monitor its body temperature using a rectal thermometer (Harvard Apparatus Ltd, Cambridge, UK.). Ophthalmic ointment was applied to the eyes to prevent corneal drying. Lidocaine drops were massaged gently into the skin of the scalp before a midline incision of approximately 2–3 cm on the scalp was made to expose the surface of the skull. The temporalis muscle contralateral to the whisker pad to be stimulated was carefully separated from the skull. A small hole (<2 mm in diameter) above the barrel cortex (2.5 mm caudal to bregma and 6 mm lateral to midline; Paxinos & Watson, 2005) was drilled into the skull and the bottom of the hole was thinned to translucency without damaging the dura.

After surgery, the rat, secured on the stereotaxic frame, was transferred to a Faraday cage mounted on top of a vibration isolation workstation. An oximeter sensor clamp connected to an oximeter control unit (MouseOxPlus, Starr Life Sciences Corp., Oakmont, PA, USA) was attached to the rat's hind paw to monitor continuously the following physiological parameters: heart rate, breath rate, arterial oxygen saturation, pulse distention and breast distention. The hard-plastic nose cone for ISO administration was then replaced with a microflex breather fitted with a transparent soft nose cone which was modified (Kang et al., 2017) to allow easy whisker stimulation to one side of the whisker pad without compromising the ISO administration. Two stainless steel stimulating electrodes were connected to an isolating current stimulator (made in-house) and then inserted into the whisker pad. A needle was used to pierce the dura to allow the insertion of a 16-channel multi-lamina recording microelectrode (100 μm spacing, area of each site 177 μm^2 , NeuroNexus Technologies, Ann Arbor, MI, USA) perpendicular to the cortical surface. This microelectrode was connected to a preamplifier that was in

turn connected to a data acquisition unit via a fibre optic cable (Tucker David Technologies Inc., Alachua, FL, USA, sampling rate 24.2 kHz). It was then slowly inserted to a depth of 1600 μm . Stimulation consisted of a pair of brief constant current pulses (1.2 mA, 0.3 ms width) with the interval between the pair varying at 100, 200 and 400 ms. It was delivered repeatedly every 10 s, or every trial. As we will only analyse spontaneous activity for this paper, details of the paired stimulus are omitted.

During neural recording, the level of anaesthesia was varied between level III3 (light), level III4 (deeper) and level IV (deep) (Friedberg et al., 1999) by changing the concentration of ISO while O_2 flow was kept at 0.5 l/min. The ISO concentrations (mean \pm SD) were level III3: $0.9 \pm 0.2\%$; level III4: $1.4 \pm 0.2\%$; and level IV: $2.3 \pm 0.1\%$. Three hundred trials per rat were collected at anaesthetic levels III3 and III4, whereas at anaesthetic level IV, one hundred trials per rat were collected.

After each experiment, the rat was terminated by deep anaesthesia at 5% ISO with an oxygen flow rate of 1 l/min for >5 min, followed by cervical dislocation.

Realignment of channels

All evoked field potential recordings were aligned with the stimulus onset at $t = 0$ s. To align the data in cortical depth, an inverse current source density (iCSD, source radius = 0.5 mm) analysis with a Gaussian filter (SD 50 μm) was applied to locate the granular (Gr) layer sink (Pettersen et al., 2006; Pettersen et al., 2008). The CSD and the corresponding LFP data were then aligned according to this sink location across animals, and the common sink was assigned to channel 7, about 600 μm below the pial surface. Thus, the absolute depth of the electrode was aligned so that channel 7 corresponded to the maximum evoked LFP. After the spatial realignment, only 11 channels (channel 3 to channel 13, covering cortical depth 0.2 to 1.2 mm) were available for analysis from all rats in this study. In the subsequent analysis, we used data from channels 3, 7 and 12 to represent the SG, Gr and IG layers, respectively (Constantinople & Bruno, 2013; Narayanan et al., 2017; Oberlaender et al., 2011; Petersen, 2007). The corresponding cortical depths of these channels are approximately 0.2 (SG), 0.6 (Gr) and 1.1 (IG) mm from the pial surface, respectively.

Estimating multi-unit activity

We estimated MUA from LFP recordings in three steps. (i) The LFP data were bandpass-filtered in the frequency range 300–5000 Hz. (ii) The filtered data were fully rectified, i.e. $x = |x|$. (iii) The rectified data was divided into 1 ms non-overlapping windows, and the MUA for each window was determined as the number of data points

above a pre-determined threshold (Devonshire et al., 2007; Martin et al., 2013) with units counts per milliseconds (cpms). In most previous studies, this threshold was calculated using the standard deviation or median of the spontaneous LFP in the absence of evoked neural responses. However, for the current study this kind of threshold estimate has two drawbacks. First, because our spontaneous LFP contains Up and Down states, the threshold would be biased by Up state spiking activity. Secondly, spontaneous spiking is significantly higher in the IG layer of the cortex (Steriade & Amzica, 1996). For multichannel LFP data, this kind of threshold calculation would result in different thresholds for different channels, which is undesirable. To estimate a single unbiased threshold reflecting the baseline ‘noise’ independent of the channels, we recorded the LFP at the deep anaesthetic level IV when no Up state was present. This provided us with data from which the MUA threshold was first calculated for every channel separately using the equation (Quiroga et al., 2004)

$$\sigma_n = \text{median} \left(\frac{|x|}{0.6745} \right) \quad (1)$$

where x is the bandpass-filtered LFP data and σ_n is an estimate of the standard deviation of the background noise. The threshold we used was $3\sigma_n$. As no significant difference between different channels was found, the average threshold across all channels was then used as the threshold value for MUA calculations.

To align the MUA of a channel by their onset in order to identify the Up state, the above MUA was first low-pass filtered at 30 Hz. The histogram of the filtered data showed a sharp peak near 0 cpms and a long tail in the range 1 to 20 cpms. An abrupt change in the slope of the histogram around 0.5 cpms was observed. Thus, the MUA data above 0.5 cpms continuously for at least 100 ms was aligned to the first time point above this threshold, defined as the onset of the Up state (Fiáth et al., 2016). We varied the threshold value between 0.5 and 1 cpms and the lowpass filter cut off frequency between 10 and 50 Hz. These variations did not qualitatively alter the resulting Up state alignment.

Classifying spontaneous LFPs into Up, Dynamic Down and Static Down states

Spontaneous LFPs were recorded from 2 to 9 s after each stimulus onset (Castro-Alamancos, 2004). We classified the spontaneous LFP into the Up, DD and SD states based on the difference signal between the SG layer LFP (LFP_{SG}) and IG layer LFP (LFP_{IG}) (Fig. 1E):

$$d(t) = LFP_{SG} - LFP_{IG} \quad (2)$$

An explanation of the characteristics of these states is given in Results. To minimise the effect of noise, the LFP data were first subsampled to 1 kHz, which included an antialiasing lowpass filter. A histogram of $d(t)$ was plotted to determine a threshold value for state classification (Fig. 1F). We observed an abrupt change in the slope of the histogram around ± 0.1 mV, indicating a separation of data surrounding $d = 0$ mV from data that deviated significantly from zero. A slight variation in this value did not qualitatively change our findings. Thus, the following criteria were used to generate a state signature $S(t)$ for each LFP time series (illustrated graphically in Fig. 1E, bottom):

$$S(t) = \begin{cases} +1 \triangleq \text{Up state} & \text{if } d(t) > 0.1 \text{ mV} \\ -1 \triangleq \text{DD state} & \text{if } d(t) < -0.1 \text{ mV} \\ 0 \triangleq \text{SD state} & \text{if } |d(t)| \leq 0.1 \text{ mV} \end{cases} \quad (3)$$

To investigate Up state initiation, we created an alignment mask M by identifying a sustained period (T_U) of only Up state, preceded by a single alignment time point (A) of a Down state (either Dynamic or Static). Data points preceding A in turn had to consist of a sustained period of either only DD (T_{DD}) or only SD (T_{SD}) state. However, in-between we allowed for a brief period (T_x) of fixed duration without any state constraints to accommodate the typically noisy transition time between states.

Thus, the alignment mask for Up state initiation from DD was

$$M_{DD \rightarrow U}^U = \left[\underbrace{-1, -1, \dots, -1}_{T_{DD}}, \underbrace{x, \dots, x}_{T_x}, \underbrace{A}_{\uparrow}, \underbrace{+1, +1, \dots, +1}_{T_U} \right], \quad (4)$$

and from SD it was

$$M_{SD \rightarrow U}^U = \left[\underbrace{0, 0, \dots, 0}_{T_{SD}}, \underbrace{x, \dots, x}_{T_x}, \underbrace{A}_{\uparrow}, \underbrace{+1, +1, \dots, +1}_{T_U} \right], \quad (5)$$

where $x = \{-1, 0, +1\}$ and $A = \{-1, 0\}$ indicate time points that can have the values in their respective sets. The arrow indicates the determined time point of alignment. Similarly, to find epochs of Up state termination, we first identified a sustained period of the Up state followed by a single time point of DD or SD state for alignment. The mask ended with a sustained period of either DD or SD state, while again allowing for a brief, fixed phase of noisy

transition. The alignment mask for Up state termination to a DD state hence was:

$$M_{U \rightarrow DD}^U = \begin{bmatrix} \underbrace{+1, +1, \dots, +1}_{T_U}, \underbrace{A}_{\uparrow}, \underbrace{x, x, \dots, x}_{T_X}, \\ \underbrace{-1, -1, \dots, -1}_{T_{DD}} \end{bmatrix}, \quad (6)$$

and to a SD state it was:

$$M_{U \rightarrow SD}^U = \begin{bmatrix} \underbrace{+1, +1, \dots, +1}_{T_U}, \underbrace{A}_{\uparrow}, \underbrace{x, x, \dots, x}_{T_X}, \\ \underbrace{0, 0, \dots, 0}_{T_{SD}} \end{bmatrix}. \quad (7)$$

The same principle was used to construct alignment masks for Down state initiation and termination. Thus, to

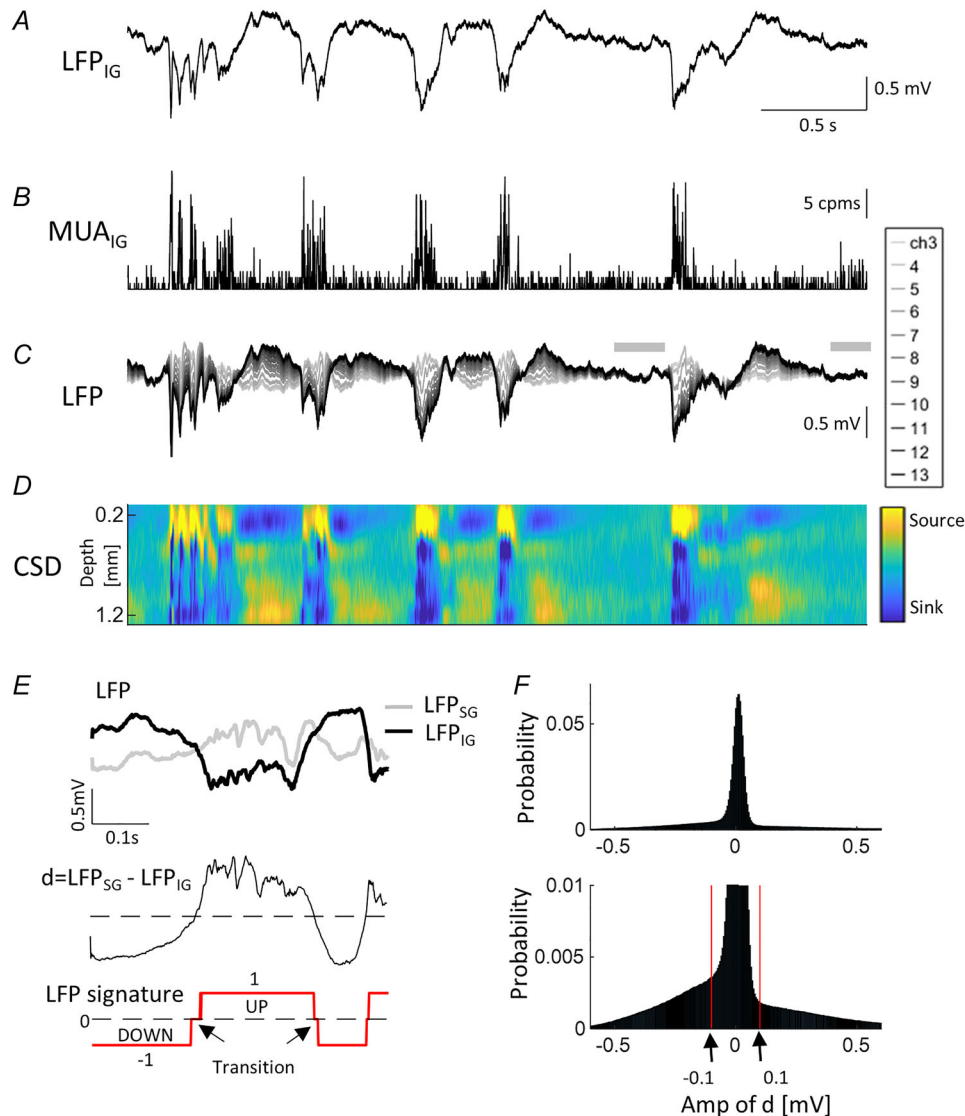


Figure 1. An example of the correspondence between local field potentials (LFPs), multi-unit activity (MUA) and current source density (CSD) during slow wave oscillations (SWOs)

A, a single channel LFP in the IG layer. B, the corresponding MUA. C, the corresponding multi-channel LFP. Grey bars indicate periods during which all LFP channels converge to baseline 0 mV. D, the corresponding CSD. E, top, superimposed LFPs from the SG layer (grey) and IG layer (black). Middle, their difference $d = LFP_{SG} - LFP_{IG}$. Bottom, the corresponding LFP signature calculated by thresholding d . F, top, normalised histogram of the difference signal d . Bottom, the same histogram zoomed in on the y-axis to show abrupt changes in the vicinity of ± 0.1 mV (red lines).

identify a DD state termination to Up state we used

$$M_{DD \rightarrow U}^{DD} = \left[\begin{array}{c} \underbrace{-1, -1, \dots, -1}_{T_{DD}}, \underbrace{B}_{\uparrow}, \underbrace{x, x, \dots, x}_{T_x}, \\ \underbrace{+1, +1, \dots, +1}_{T_U} \end{array} \right], \quad (8)$$

where $B = \{0, +1\}$, and to SD state

$$M_{DD \rightarrow SD}^{DD} = \left[\begin{array}{c} \underbrace{-1, -1, \dots, -1}_{T_{DD}}, \underbrace{B}_{\uparrow}, \underbrace{x, x, \dots, x}_{T_x}, \\ \underbrace{0, 0, \dots, 0}_{T_{SD}} \end{array} \right]. \quad (9)$$

Similarly, DD state initiation from the Up state has mask

$$M_{U \rightarrow DD}^{DD} = \left[\begin{array}{c} \underbrace{+1, +1, \dots, +1}_{T_U}, \underbrace{x, \dots, x}_{T_x}, \underbrace{B}_{\uparrow}, \\ \underbrace{-1, -1, \dots, -1}_{T_{DD}} \end{array} \right], \quad (10)$$

and from the SD state

$$M_{SD \rightarrow DD}^{DD} = \left[\begin{array}{c} \underbrace{0, 0, \dots, 0}_{T_{SD}}, \underbrace{x, \dots, x}_{T_x}, \underbrace{B}_{\uparrow}, \\ \underbrace{-1, -1, \dots, -1}_{T_{DD}} \end{array} \right]. \quad (11)$$

The fixed transition period T_x was set to 10 ms if changing to an Up state, but 20 ms for changing to a DD or SD state, because inspection of our data suggested that the latter transition was slower than the former. Variations by ± 2 ms of these durations did not produce qualitatively different results. To obtain robust state transitions, we used a minimum of 80 ms for T_U , T_{DD} and T_{SD} , during which the LFP data must stay entirely in the respective state for the segment to be classified accordingly. Note that for example $M_{DD \rightarrow U}^U$ and $M_{DD \rightarrow U}^{DD}$, eqns (4) and (8) are very similar in considering the same kind of transition, indicated by the subscript, but differ in the selection of the alignment point, indicated by the superscript. Furthermore, we have also computed the SD masks $M_{SD \rightarrow U}^{SD}$, $M_{SD \rightarrow DD}^{SD}$, $M_{U \rightarrow SD}^{SD}$ and $M_{DD \rightarrow SD}^{SD}$. Their form can be derived straightforwardly from eqns (8)–(11) by exchanging throughout labels $DD \leftrightarrow SD$ and

the corresponding mask values $-1 \leftrightarrow 0$, with in particular an alignment point $C = \{-1, +1\}$. However, these did not contribute additional information for our analysis and results are neither shown nor discussed in the following.

Single-unit activity analysis

We extracted single unit activity (SUA) from the four IG layer channels (10/11/12/13) of the 16-channel laminar microelectrode. For each individual animal, we concatenated the four channels of wide band LFPs recorded over continuously recorded trials (between 100 and 300 trials), and the resultant data were analysed together. Next, the data were processed for ‘spike sorting’ using custom software, as previously described (Csicsvari et al., 1998; Csicsvari et al., 1999; O’Neill et al., 2017). Briefly, the concatenated signals were digitally high-pass filtered (0.8–9 kHz) and the power (root mean square) of the filtered signal was computed in a sliding 0.2 ms window. Any event with a power > 5 SD of the baseline was identified as a spike and the waveform extracted. The resultant waveforms were then reconstructed at 40 kHz and aligned to the up-sampled peak. These wave form shapes were then compressed into three features, using principal component analysis. Because each recorded spike could be recorded on up to four channels, a given spike could be identified using a 12-dimensional feature vector. Using these data, spikes were then automatically sorted into putative single units using Klustakwick 3.0.2 (Harris et al., 2001), the results of which were then manually curated using custom-made ‘cluster cutting’ software (Csicsvari et al., 1999). Only units with clear refractory periods in their autocorrelation as well as defined cluster boundaries were kept for further analysis. Cluster separation was confirmed by calculating the Mahalanobis distance (Harris et al., 2001) between each pair of clusters, as well as through visual inspection for a lack of common refractory period in cell-pair cross-correlations.

For each cell identified, spike sequences were time-aligned to the $DD \rightarrow U$ or $SD \rightarrow U$ transitions. Epochs without the presence of action potentials were excluded, and the spike rate for each cell was calculated by summing all spike activities over 5 ms non-overlapping windows across all epochs, normalised by the number of epochs involved. The onset of the first spike in a train was calculated by finding the first non-zero time bin in the range -50 ms before the time of alignment to 100 ms after. To find the maximum spike rate per cell, spike trains were smoothed using a Gaussian weighted average (MATLAB (The MathsWork, Natick, MA, USA) function ‘smoothdata’) with a window of 30 ms before the maximum was calculated.

Data selection, rate of state transition, and statistical analysis

The data presented here were collected in an ageing study which included rats from three age groups (pre-adolescence, young adult and middle-aged adult). Evoked LFPs were analysed and published in Kang et al. (2020). Here we focussed our analysis on the spontaneous LFP responses under the anaesthetic level III3, during which the LFP displayed oscillatory characteristics at frequencies around 2 Hz. Only data from the young adult group were used, and 3 out of 10 rats in this group were excluded from the analysis due to high frequency noise in the data that interfered with the MUA analysis. Thus, data from seven rats were analysed throughout this paper unless stated otherwise.

All LFP and MUA data analysis was performed in MATLAB. During state transitions between DD \rightarrow Up and SD \rightarrow Up states, the LFP_{IG} typically displayed a sharp decrease in its amplitude. The slope of this decrease was calculated from LFP_{IG} within a 15 ms window, including 5 ms pre and 10 ms post the time of alignment. A straight line was fitted to the data (MATLAB function 'polyfit', order = 1) and the slope of the fitted line was taken as the rate of transition. The same process was used to calculate the rate of state transition for the MUA data and for the Up \rightarrow DD transition except that for the latter, the 15 ms window was taken 10 ms pre and 5 ms post the time of alignment.

For each state transition, the number of epochs identified per animal was different. The mean, standard deviation and the number of epochs per animal and per condition are reported for all seven animals in the accompanying Statistical Summary Document. To compare the rate of transition between DD \rightarrow Up and SD \rightarrow Up states, a paired-sample Student's *t*-test was used when the duration of the preceding Down state was ≥ 100 ms. We further classified the preceding Down state into three specific durations and used a two-way repeated measures ANOVA (MATLAB function 'RMAOV2'; Huck, 2008) to compare the slopes across the two transitions over three durations. For the Up \rightarrow DD transitions over three different Up state durations, the transition slopes were compared using a one-way repeated measures ANOVA (MATLAB function 'RMAOV1'; Huck, 2008). For SUA analysis, two sets of spike onset times were tested for equal variance using the *F*-test (MATLAB function 'vartest2').

All data using paired-samples *t*-tests were first checked for normality (MATLAB function 'jbtest') before testing for significance. For DD \rightarrow Up vs. SD \rightarrow Up comparisons, the effect size was calculated using the difference between the means to be compared normalised by the standard deviation of the variable under the DD \rightarrow Up condition.

Results

Spontaneous down states consisted of dynamic and static states with distinct CSD characteristics

Under anaesthetic level III3, LFP recordings displayed typical SWO characteristics. If only the LFP_{IG} was plotted (Fig. 1A), it showed a sequence of positive and negative deflections, with the corresponding MUA (Fig. 1B) indicating that negative deflections were associated with intense spiking activity (Up state), while positive deflections were associated with baseline activity (Down state). When multi-channel LFP was displayed, we observed additional characteristics of these recordings. First, the multi-channel traces were enveloped by LFP_{SG} and LFP_{IG} (Fig. 1C and E top). This envelope was dominated by two alternating states: (i) LFP_{SG} > LFP_{IG} during the Up state, and (ii) LFP_{SG} < LFP_{IG} during the Down state, as shown by many previous studies of SWOs (Chauvette et al., 2010; Fiáth et al., 2016; Steriade & Amzica, 1996). Secondly, for longer Down states, multi-channel LFP recordings converged towards baseline (0 mV) and became indistinguishable from each other (Fig. 1C, grey bars), a characteristic not easy to observe if only a single channel LFP was displayed. Finally, although MUA remained at baseline throughout a prolonged Down state, CSD showed strong sources in the Gr and IG layers, and a sink in the SG layer during the initial Down state, a dipole configuration which has the reverse polarity from that during the Up state (Fig. 1D). But the source/sink activities disappeared during the later phase of the Down state when multi-channel LFP converges. These observations from our data raise the following questions: What are the mechanisms underlying the generation of the dipole during the Down state? Why is the polarity reversed from that of the Up state? What determines the temporal duration of this dipole? To investigate this and to be more precise with our terminology, we define the Down state with depth-positive LFP and the presence of CSD sinks and sources as the DD state, and the Down state without CSD sources and sinks as the SD state.

The sequence of Up, DD and SD states is not random

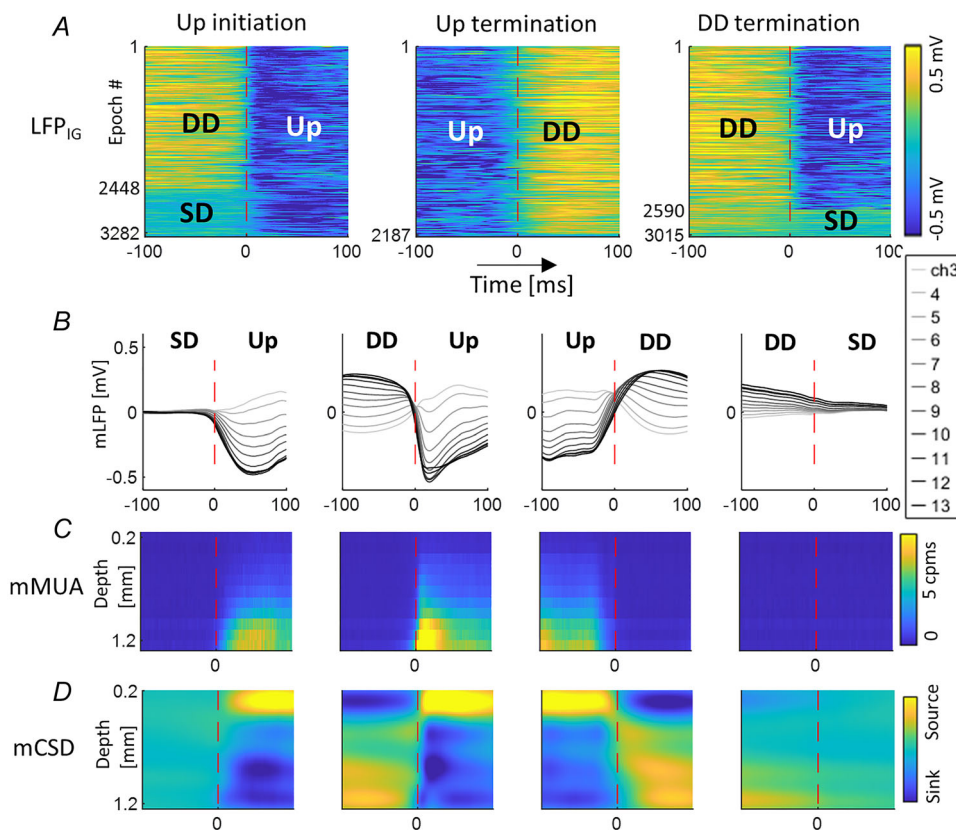
We first studied the sequence of occurrence of the Up, DD, and SD states to see if it was random or followed specific patterns. A major difficulty in examining different states robustly in spontaneous LFP is that these fluctuations are not time-locked, unlike evoked LFPs, which can be aligned to the stimulus onset. In addition, we could not use MUA onset to align LFP data in this study because MUA could not distinguish between the DD and SD states. To resolve this, we used the difference signal

Table 1. Number of epochs identified for state transitions

Up initiation		Up termination		Down initiation		Down termination	
DD → Up	2448 (74.6%)	Up → DD	2156 (98.6%)	Up → DD	2473 (99.4%)	DD → Up	2590 (85.9%)
SD → Up	834 (25.4%)	Up → SD	31 (1.4%)	SD → DD	15 (0.6%)	DD → SD	425 (14.1%)

$d = \text{LFP}_{\text{SG}} - \text{LFP}_{\text{IG}}$ and designed masks eqns (4)–(11) with the state signature eqn (3) to obtain alignment time points (see Methods). This enabled us to investigate transitions between different states without making *a priori* assumptions about the order of occurrence of these states. We observed that the two most unlikely transitions were Up → SD (1.4%) and SD → DD (0.6%) (Table 1). A closer examination of the epochs in these transitions revealed that most epochs would be eliminated by reducing the threshold for d during the classification. This result showed that transitions between states were strongly dominated by either Up → DD → SD → Up or Up → DD → Up (Fig. 2A).

We then plotted the mean LFP (mLFP) across cortical depth for the transitions SD → Up, DD → Up, Up → DD and DD → SD, respectively (Fig. 2B) and computed the mean MUA (mMUA) (Fig. 2C) and mean CSD (mCSD) (Fig. 2D) for each transition. Note that because LFP was averaged over epochs, fast dynamics, as observed in individual epochs, were smoothed out, and mLFP contains only lower frequency potential changes. Furthermore, because Down state initiation was very similar to Up state termination, it was not included in Fig. 2. As expected, MUA could not distinguish between DD and SD states, but the mCSD maps for the three states were distinct; the Up and DD states showed source–sink

**Figure 2. Transitions between different states**

A, IG layer LFP during Up state initiation (left), Up state termination (middle), and DD state termination (right). The Up state can be preceded by both DD and SD states. The DD state can be terminated by both Up and SD states. However, the Up state is terminated overwhelmingly by the DD state. B, mean multi-channel LFP for transitions (left to right panels): SD → Up (number of epochs $n = 834$), DD → Up ($n = 2448$), Up → DD ($n = 2156$), and DD → SD ($n = 425$), respectively. C, corresponding mean MUAs. D, corresponding mean CSDs. A red dashed line marks the time of alignment throughout.

activities with opposite polarity, but the SD state showed no sinks and sources. The reversal of polarity in the CSD map between the Up and DD states have been observed previously (Chauvette et al., 2010; Steriade & Amzica, 1996). We will re-examine the polarity reversal phenomenon in detail in the Discussion.

To ensure that results from our classification method using LFPs were similar to those using MUA to classify Up states, we used an alternative method (Fiath et al., 2016) by aligning MUA first, and then collecting the corresponding LFP data 100 ms pre and post the time of alignment. The two MUA maps (Fig. 3, bottom two panels) were compared by calculating the peak and the mean IG layer MUAs from the two methods. We found a significant difference in the peak values ($P = 0.0192$, paired-samples t -test), suggesting that the peak MUA calculated by aligning the MUA onset (mean \pm SD = 5.863 ± 2.089 cps) was smaller than that by aligning through LFP data (6.7745 ± 0.900 cps). This was as expected because the latter alignment included only DD \rightarrow Up transitions whereas the former could not distinguish between the DD \rightarrow Up and the SD \rightarrow Up transitions (see next section). But we did not find significant difference in the time-averaged MUA ($P = 0.941$) over the time range $[-50 \text{ } 100]$ ms with respect to the time of alignment

($t = 0$), suggesting that the two methods of estimating MUA provided similar population spiking activities over time.

The multi-channel mLFP obtained using the alternative alignment method was also similar to that from our DD \rightarrow Up analysis (Fig. 3, top panels). However, the Down state multi-channel LFP using the alternative alignment (Fig. 3B, top) showed less variation between channels than our DD \rightarrow Up (Fig. 3A, top) because it does not distinguish between the two transitions DD \rightarrow Up and SD \rightarrow Up.

Initiation of the Up state was faster from DD than from SD states

In the analysis of Up state initiation, we noticed that mLFP_{IG} appeared to transition faster from DD \rightarrow Up than from SD \rightarrow Up (Fig. 2B, left two panels). Closer examination of the slopes of LFP_{IG} and the corresponding MUA_{IG} for each rat confirmed this observation (Fig. 4A and B). We subsequently calculated mean slopes of the LFP_{IG} and MUA_{IG} for each animal during the two transitions (Fig. 4C and D, see also Statistical Summary Document, Questions 1 and 2, respectively). Paired-sample t -tests showed that the slope of transition for DD \rightarrow Up was indeed faster than for SD \rightarrow Up for both LFP_{IG} ($P = 2.29 \times 10^{-6}$) and MUA_{IG} ($P = 5.81 \times 10^{-5}$), with effect sizes 5.74 and 0.811, respectively. We further noted that the onsets of the MUA for the two transitions were different, with an early onset (mean \pm SD = -7.43 ± 1.72 ms) for DD \rightarrow Up, whereas for SD \rightarrow Up, the onset (4.57 ± 2.23 ms) was significantly delayed ($P = 5.98 \times 10^{-17}$, paired-sample t -test, effect size 6.98).

We suspected that the slope of transition may depend on the duration of the preceding state, and thus we decided to further classify the transition data into different groups based on the duration of the preceding Down state (DD or SD). To decide the appropriate lengths of these durations, we computed histograms for the duration of the DD and SD state preceding an Up state (Fig. 5A and B), as well as the duration of the Up state preceding a DD state (Fig. 5C). Figure 5A shows that 90.0% of the epochs for the DD \rightarrow Up transition had DD duration < 250 ms. Furthermore, Up states tended to have shorter durations, with 87.5% of the Up \rightarrow DD transitions having Up state durations < 200 ms. The histograms also showed that SD appeared less frequent than the other two states, because at anaesthetic level III3, the LFP temporal profiles mostly switched between positive and negative deflections. Only sometimes was this interleaved with a brief quiescent state (Fig. 1C) that rarely could last up to several seconds.

It is worth noting that although SWOs have been observed across humans and animals, when awake, under anaesthesia and during sleep, the frequency of SWOs

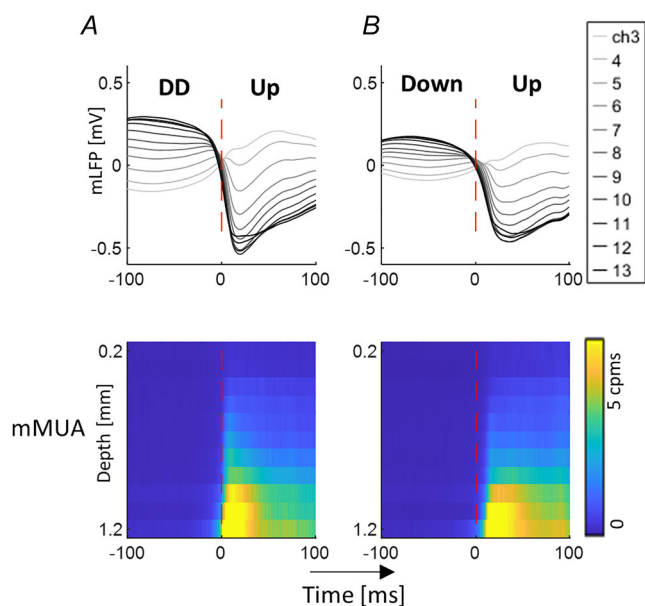


Figure 3. Comparison of Up state initiation calculations

A, Up state initiation from DD state calculated using eqn (4), with the time of alignment (red dashed line) determined by thresholding the difference between LFP_{SG} and LFP_{IG}. Top, mean multi-channel LFP ($n = 2448$). Bottom, the corresponding MUA across cortical depth. B, Up state initiation from Down state (regardless whether DD or SD) calculated by thresholding the filtered MUA in the IG layer. Top, the mean multi-channel LFP ($n = 4189$). Bottom, the corresponding MUA across cortical depth.

depends on species and wakefulness/anaesthetic regimes (Kroeger & Amzica, 2007; Mizuseki et al., 2011; Steriade et al., 1993; Torao-Angosto et al., 2021). Thus, the durations of the different states presented here reflects specifically our anaesthetic regime (rats under ISO).

Based on the histograms, we re-grouped the transition data into three classes so that the duration (including a brief 10 ms transition period) of the preceding DD or SD

state was (200 250] ms, (150 200] ms and (100 150] ms, respectively (Figs 6A and C). Note that the interval (a, b] for some x means $a < x \leq b$. This ensured that no epoch was classified more than once.

When the mean LFP_{IG} for the three classes were super-imposed, changing the duration of the preceding state did not change the speed of Up state initiation (Fig. 6E, left panel). The main determining factor for the speed

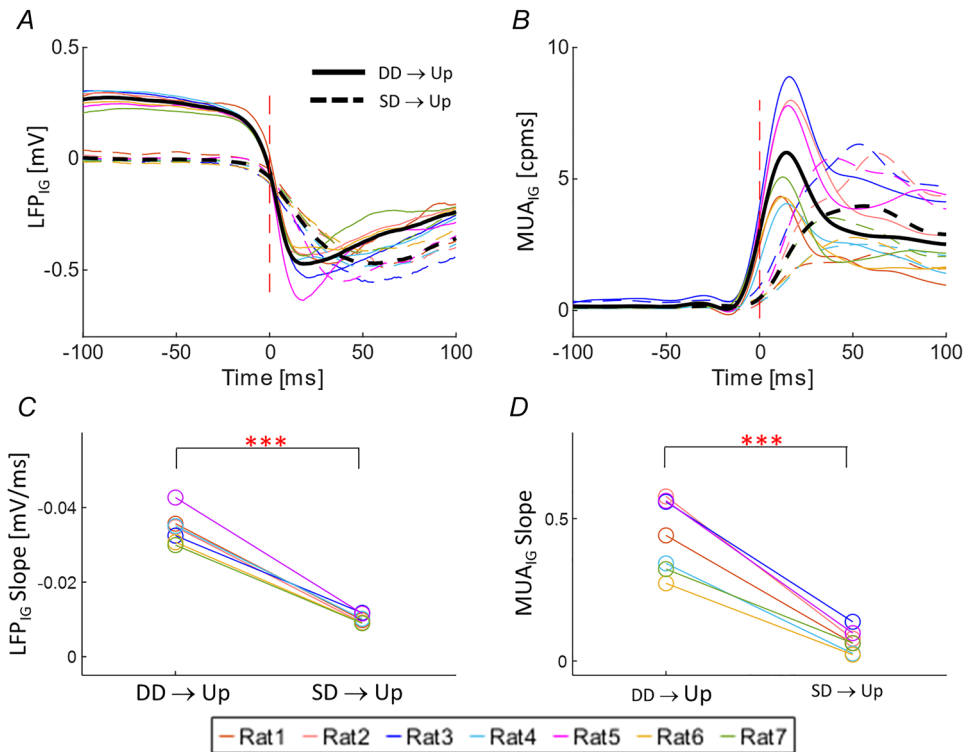


Figure 4. Comparison of LFP_{IG} and MUA_{IG} for Down to Up state transitions (averaged per animal, $n = 7$)
 A, individual averaged animal LFP_{IG} (coloured) and grand average LFP_{IG} (black) for DD → Up (continuous curves) and SD → Up (dashed curves) state. B, the corresponding MUA_{IG}. The red dashed line marks the time of alignment. C, the LFP_{IG} slopes of each animal under DD → Up vs. SD → Up transitions. D, the corresponding slopes of state transitions for MUA data. (***) $P < 0.001$.

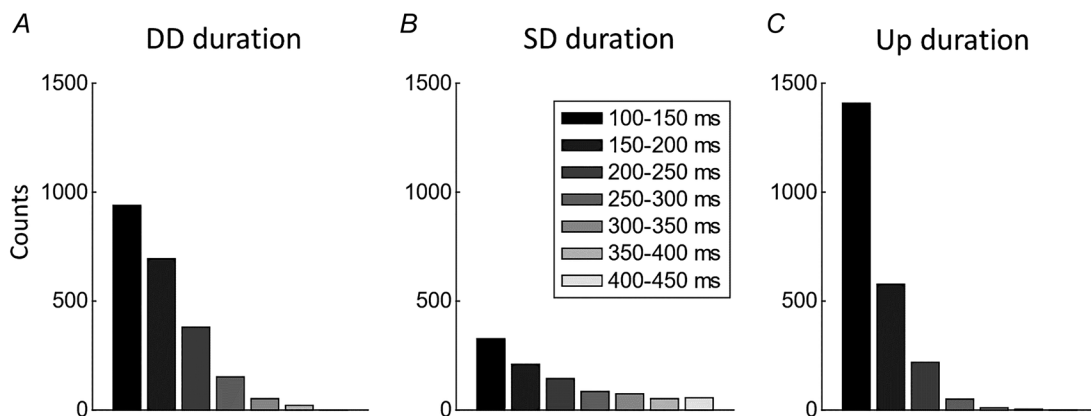


Figure 5. Histograms of the durations of states
 A, histogram of the duration of DD states preceding an Up state. B, histogram of the duration of SD states preceding an Up state. C, histogram of the duration of the Up states preceding a DD state.

of transition was whether the preceding Down state was dynamic or static. We then computed the corresponding CSD for each condition (Fig. 6B and D) and observed that for the DD → Up transition, there was an earlier but brief sink in the IG layer immediately after the time of alignment, followed by a second prolonged sink. This

earlier sink was absent in the SD → Up transition. To reveal the nature of the fast sink more clearly, we superimposed the CSD time courses in the IG layer over different durations of DD (Fig. 6E middle) with an arrow pointing to the fast sink, and different durations of SD (Fig. 6E right) where no early sink was present.

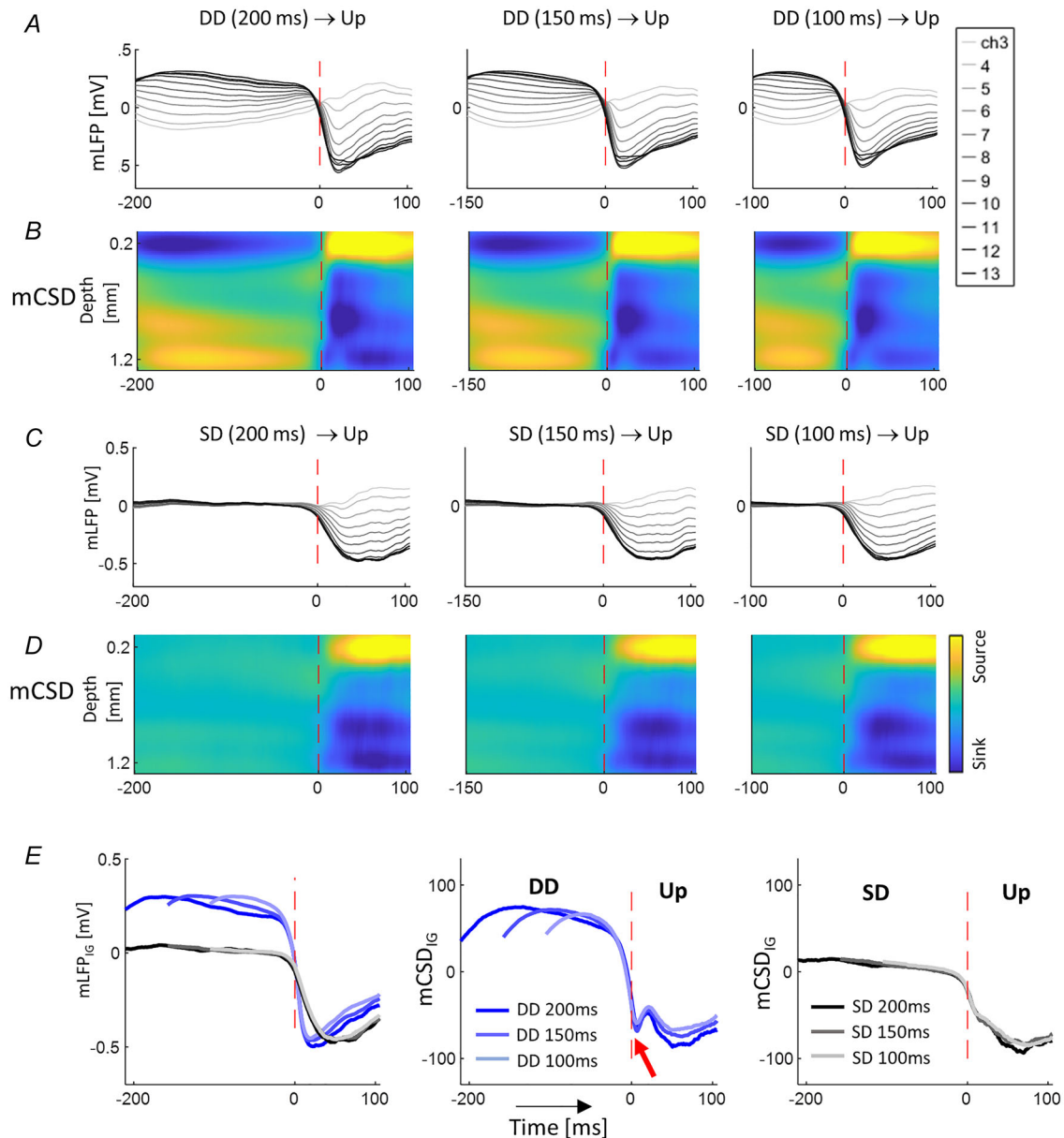


Figure 6. Up state initiation from Down state with different Down state durations

A, mean LFP for DD → Up for different durations of the DD state. (Left, Down state duration (200–250) ms, number of epochs $n = 402$; middle, Down state duration (150–200) ms, $n = 724$; right, Down state duration (100–250) ms, $n = 985$.) B, the corresponding mean CSD maps. C, mean LFP for SD → Up for different durations of the SD state. Same durations as for DD. (Left: $n = 150$; middle: $n = 219$; right: $n = 339$.) D, the corresponding mean CSD maps. E, left, comparison of the mean LFP_{IG} during DD → Up (blue lines) and SD → Up (grey lines). Middle, the corresponding mean CSD time series in the IG layer during DD → Up. The red arrow points to an initial fast sink during the Up state, followed by a slower but more prominent sink. Right, the corresponding mean CSD time series in the IG layer during SD → Up. The fast sink observed in the DD → Up transition is absent. A red dashed line marks the time of alignment throughout.

We further observed that the amplitude of the $mLFP_{IG}$ and $mCSD_{IG}$ continued to decay towards baseline during the DD state, but with little impact on the initiation of the Up state. We will return to this in the Discussion.

We subsequently calculated slopes of transitions of the LFP_{IG} from DD \rightarrow Up and SD \rightarrow Up, respectively, for each animal under each of the three different Down state durations (Fig. 7A, see also Statistical Summary Document, Question 3) and conducted a

two-way repeated measures ANOVA across the two transitions under three different preceding Down state durations. The analysis confirmed that the rate of transition DD \rightarrow Up was significantly faster than SD \rightarrow Up ($P = 1.46 \times 10^{-6}$). However, there was no significant difference in LFP slopes between Down state durations ($P = 0.109$), and no significant interaction between state transition and Down state duration ($P = 0.284$). *Post hoc* paired-samples *t*-tests showed that slopes of transition

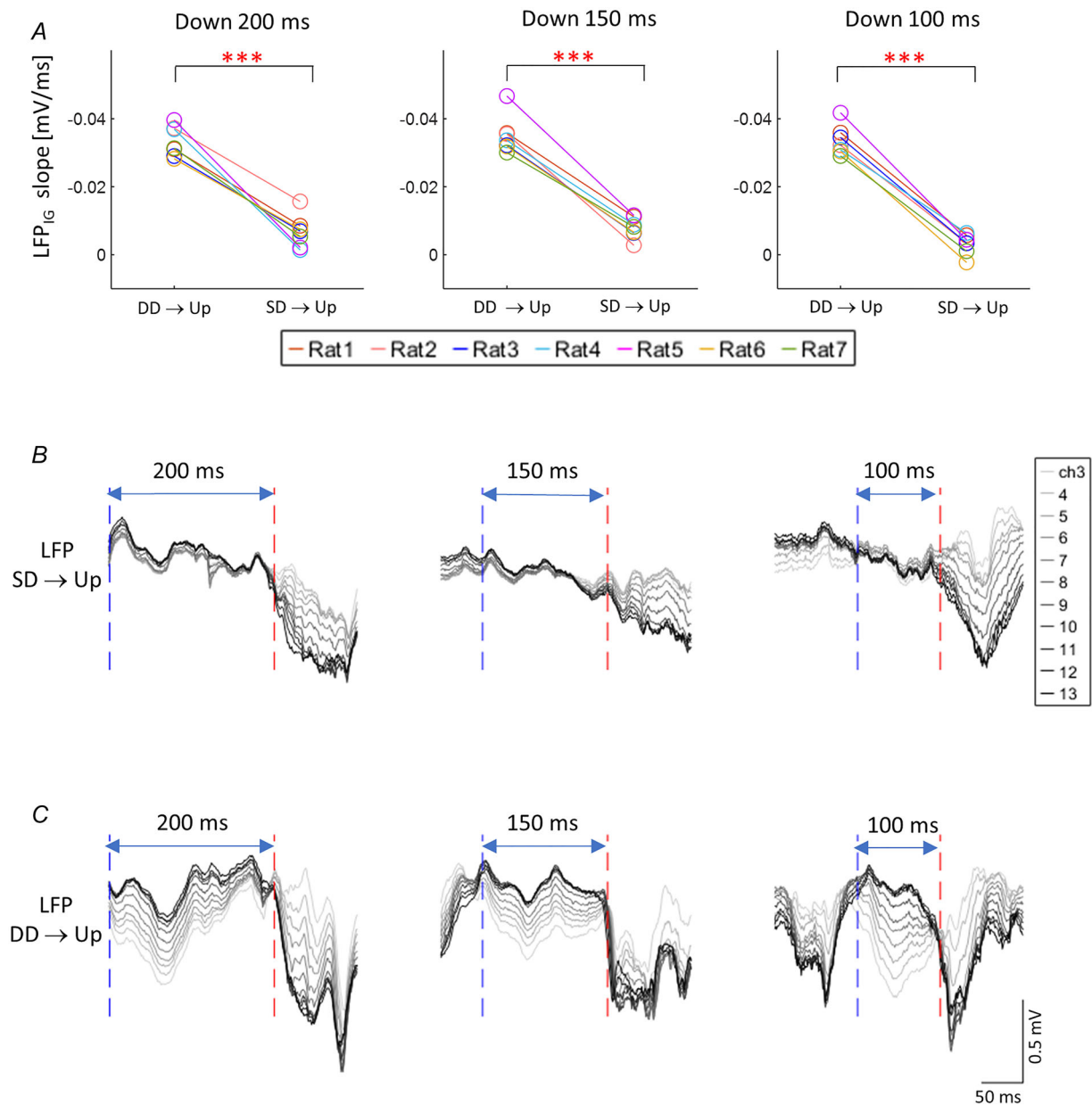


Figure 7. LFP transition from Down (DD or SD) to Up state with different Down state durations

A, comparing the LFP_{IG} slopes of each animal during DD \rightarrow Up vs. SD \rightarrow Up transitions, for preceding Down state duration (200–250 ms (left), 150–200 ms (centre), 100–150 ms (right), respectively). B, three representative SD \rightarrow Up LFPs for three different durations of the SD state. C, three representative DD \rightarrow Up LFPs for three different durations of the DD state. A red dashed line marks the time of alignment throughout. A blue dashed line marks the start of the preceding state.

during DD → Up were significantly steeper than those during SD → Up for all three durations ($P = 5.75 \times 10^{-5}$, 5.73×10^{-6} and 1.04×10^{-6} , respectively).

A representative set of LFPs show how during the transition SD → Up the amplitude of LFPs tended to increase incrementally (Fig. 7B), similar to previous observations of membrane potentials of individual neurons during the transition from Down to Up state (Chauvette et al., 2010). On the other hand, for the LFP profile during the DD → Up transition, the preceding DD state appeared to be disrupted more abruptly near the onset of the transition (Fig. 7C).

Delayed synchrony of spike onset with respect to LFP deflection during SD → Up compared with DD → Up transition

One possible explanation for the slow kinetics of the SD → Up transition would be the quantal spontaneous release of the neurotransmitter glutamate,

reflected in two types of small and low rate excitatory post-synaptic potentials (EPSPs), namely action potential (AP)-dependent spontaneous EPSP (sEPSP) and AP-independent miniature EPSP (mEPSP) (Wuarin & Dudek, 1993; Ye et al., 2010). If the mEPSP was part of the mechanism for the initiation of the Up state from the SD state, we would expect a delayed spiking activity onset during the SD → Up transition.

To investigate this, we performed an SUA analysis and extracted spiking activity from 23 cells using four linear-spaced channels from the IG layer LFP recordings (channels 10/11/12/13). The spike trains were then aligned to the DD → Up and SD → Up transitions. Overall, the probability of cell firing was higher during DD → Up compared with SD → Up (Table 2), reflected in APs present in more DD → Up epochs.

We then calculated the onset times of spike trains for all cells and found that, for 22 out of 23 cells, the first AP during the DD → Up transition occurred earlier than that during the SD → Up transition (Fig. 8A, only cell 13 has the same onset time under the two transitions).

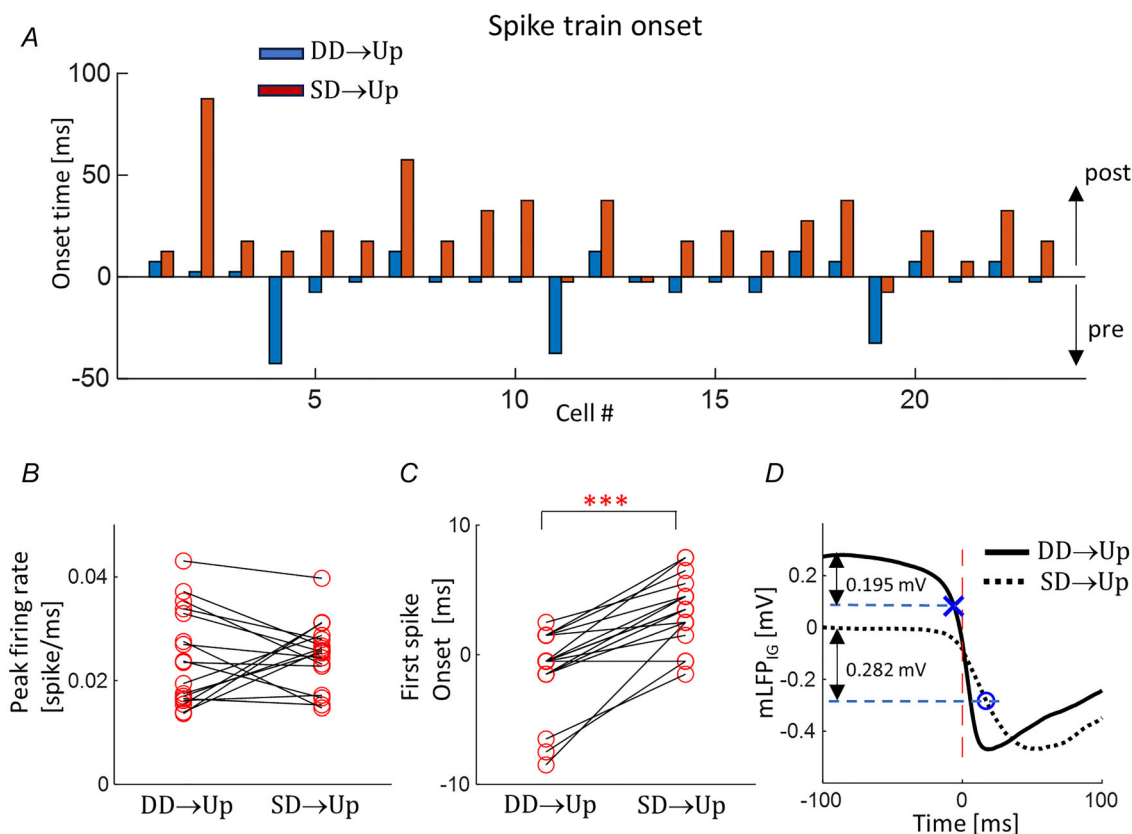


Figure 8. Comparison of single unit activity onset times

A, comparison of the first spike onset times across all cells ($n = 23$) during DD → Up (blue) and SD → Up (red) transitions. Onset times were calculated with respect to the time of alignment ($t = 0$). B, comparing the peak firing rate of cells ($n = 17$) during DD → Up (left) vs. SD → Up (right) transitions. C, comparing the first spike onset times of cells ($n = 17$) during DD → Up (left) vs. SD → Up (right) transitions. D, the mean spike rate onset times across cells ($n = 17$) during DD → Up (blue cross) and SD → Up (blue circle) transitions, respectively superimposed to the $mLFP_{IG}$ under the two conditions. The red dashed line marks the time of alignment. (***) $P < 0.001$.

Table 2. Number of epochs each identified cell is activated during the DD → Up and SD → Up transitions, respectively

Cell ID	Rat ID	No. of epoch DD → UP	No. of epoch SD → UP
1	1	57	53
2	2	50	2
3	2	38	6
4	2	109	13
5	2	78	11
6	2	42	6
7	2	21	2
8	2	267	33
9	2	94	8
10	2	87	11
11	3	144	39
12	3	40	4
13	3	65	25
14	3	72	13
15	3	77	22
16	3	51	13
17	4	120	19
18	4	53	24
19	4	411	100
20	5	38	11
21	6	42	45
22	7	26	27
23	7	84	41

Specifically, most onset times during the SD → Up transition occurred after the time of alignment. To minimise noise, we excluded all cells that were activated in less than 10 epochs under either DD → Up or SD → Up transitions, resulting in 17 cells from which we also calculated the maximum firing rate for each cell under the two transitions (Fig. 8B). No significant difference between peak firing rates was found ($P = 0.828$), suggesting that when a cell was activated, its peak firing rate was independent of the preceding Down state.

We subsequently compared the mean AP onset times during the two transitions (mean \pm SD = -6.3 ± 16.2 ms for DD → Up and 16.9 ± 13.2 ms for SD → Up respectively, Fig. 8C) and found them to be significantly different ($P = 1.75 \times 10^{-6}$, effect size 1.44). However, the variances of the two onset times were not significantly different ($P = 0.430$). When superimposed onto the mean LFP_{IG} time series (Fig. 8D), we observed that during the SD → Up transition, the mean spike onset time occurred halfway through the mLFP_{IG} negative deflection (marked by the blue circle), when mLFP_{IG} amplitude change (0.282 mV) was 60.3% of its peak change with respect to the SD baseline (calculated by averaging the first 50 ms of the mLFP_{IG} data, i.e. from -100 to -50 ms in Fig. 8C). This is in contrast to the mean spike onset time

during the DD → Up transition when it occurred in the earlier phase of the mLFP_{IG} negative deflection (marked by the blue cross), at which point the mLFP_{IG} amplitude change (0.195 mV) was only 26.1% of the peak with respect to its baseline. This delayed coupling of spiking onset to the LFP_{IG} deflection implies that mechanisms underlying the SD → Up transition may be different from DD → Up. Together with the delayed onset of the MUA during the SD → Up transition, they suggest that the AP-independent mEPSPs may play a key role in Up state initiation from the SD state (see Discussion).

Rate of transition from Up to DD was independent of the Up state duration

We further examined if the duration of the Up state could affect the rate of transition of the LFP to the DD state, as the LFP amplitude tended to decrease during the Up state. As most Up states lasted less than 200 ms (Fig. 5C), we classified the duration of the Up state into three groups: (100, 125] ms, (125, 150] ms and (150, 175] ms, making sure that no epoch was classified in more than one group, and that all Up states were terminated by a DD state lasting at least 100 ms (Fig. 9A). Similar to our previous findings, the rate of change of mLFP_{IG} during the transition seemed to be independent of the preceding Up state duration (Fig. 9B). We subsequently compared the slopes of transitions under the three Up state durations and conducted a one-sample repeated measure ANOVA, confirming that there was no significant difference between them ($P = 0.873$, Fig. 9C, see also Statistical Summary Document, Question 4.)

Next, we re-aligned the mLFP_{IG} to the respective first time points of their Up states (Fig. 9D). For comparison we show (Fig. 9E) similarly treated mLFP_{IG} for the Up state initiation from DD states of various durations (see Fig. 6E, left panel for these data before re-alignment). In both cases, we observed that the mLFP_{IG} for different durations had similar initial amplitudes and rates of decay towards baseline before they were disrupted at different time points by the beginning of the state transition.

DD states precede sustained SD states, subsequently 'disrupted' by Up states

To further demonstrate that the three states UP, DD and SD did not occur randomly, we looked at sustained SD states with duration >1 s and collected data 100 ms preceding and following such a quiescent period in the network without any additional constraints on the pre- and post-SD data. We then plotted the average in each case (Fig. 10, $n = 224$ pre, $n = 237$ post; SD duration displayed for 500 ms only) and found that the average data preceding a sustained SD state were dominated by the DD state, in

contrast to those post-SD when the average data showed dominant features of the Up state as confirmed by LFP profiles (Fig. 10A), the MUA (Fig. 10B) and the CSD maps (Fig. 10C).

Discussion

Depth-negative and depth-positive LFPs (or EEGs) recorded from the neocortex are widely used to characterise the Up and Down states observed during spontaneous SWOs. Here we have shown that for

prolonged Down states, a depth-positive LFP is followed by a 'zero' LFP (around 0 mV), with the former associated with a dipole whose polarity is opposite to that during the Up state, but the latter not showing any associated sinks and sources. We propose that the LFP patterns during SWOs reflect the alternating dominance of synaptic excitation and inhibition of local pyramidal neurons. Before we present our arguments, it is important that we make a distinction between mechanisms underlying the Up and Down states and those underlying positive and negative deflections in extracellular field potential

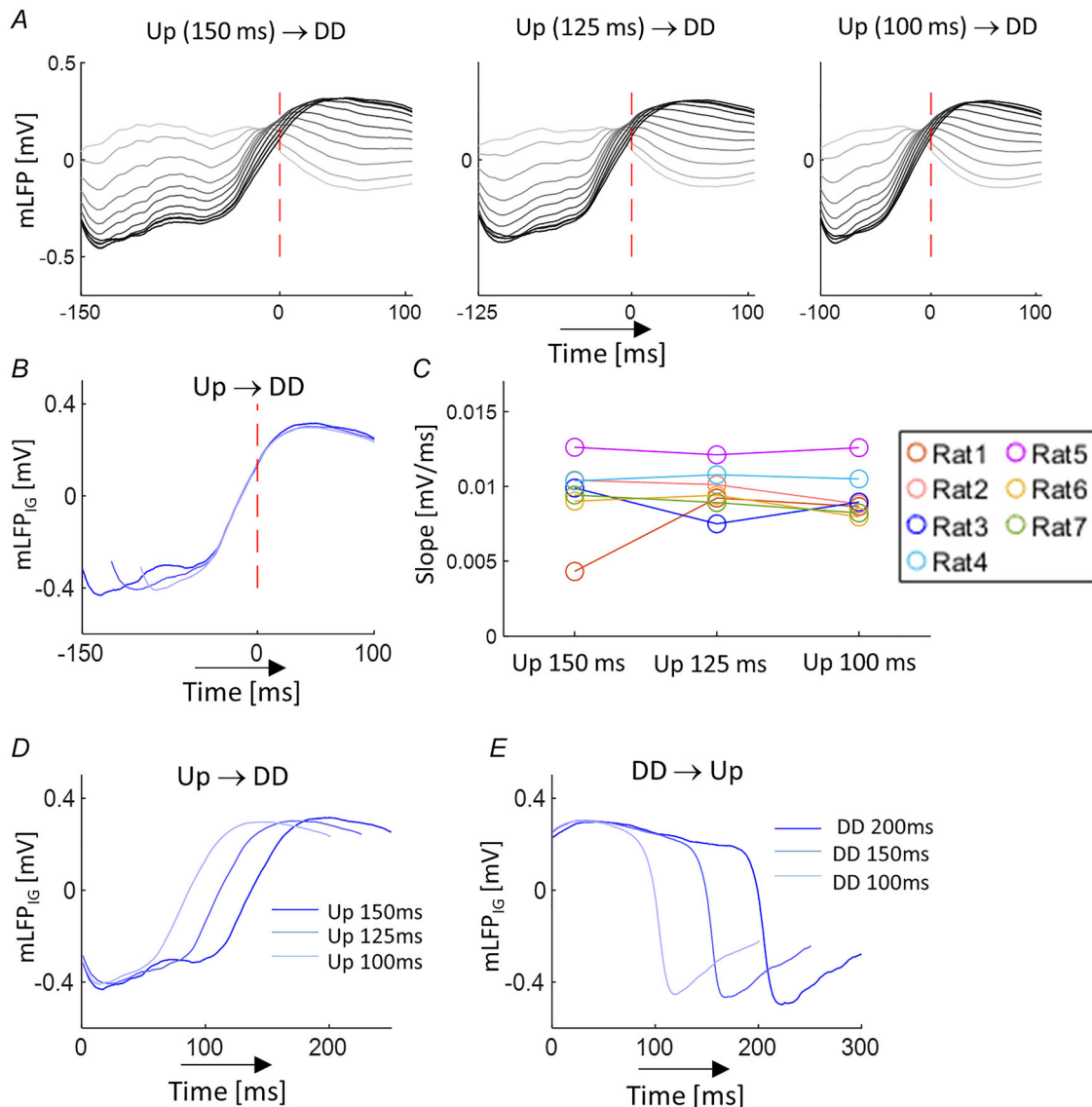


Figure 9. Up state termination and state transition re-alignment

A, mean multi-channel LFP for Up → DD transition for different durations (T_U) of the Up state. (Left: Up state duration (150–175), number of epochs $n = 361$; middle: Up state duration (125–150), $n = 546$; right: Up state duration (100–125), $n = 928$.) B, comparison of the mean LFP_G during Up → DD with LFPs aligned to the start of the DD state. C, comparison of the LFP_G slopes calculated for each animal ($n = 7$) during the three transitions. D, as in B, but with LFPs aligned to the start of the Up state. E, comparison of the mean LFP_G during DD → Up with LFPs aligned to the start of the DD state. A red dashed line marks the time of alignment throughout.

recordings during spontaneous SWOs. The former is likely to involve a complex array of cellular and network processes at different temporal scales, not all of which are distinguishable by LFP measurements. For example, the activation and deactivation of ligand- and voltage-gated channels along pyramidal neurons play important roles in the generation of the Up and Down state, controlling the type and the magnitude of transmembrane currents. However, if a class of such channels is approximately uniformly distributed along neocortical pyramidal neurons, the associated transmembrane current will not induce a prominent dipole configuration extracellularly. Hence these transmembrane currents will be unlikely to affect the temporal profile of the LFP. In addition, any transmembrane current returning to baseline much faster than the duration of the depth-positive LFP deflection observed in our data during the DD state is unlikely to explain the LFP deflections under this state.

Previous studies have demonstrated that the temporal profile of the LFP in the neocortex reflects primarily the transmembrane currents of local pyramidal neural populations and the layered structure of the neocortex (Buzsáki et al., 2012; Einevoll et al., 2013; Logothetis, 2003; Mitzdorf, 1985). In this discussion we will first re-examine

the kinetics of some of the voltage-gated channels and their possible contribution to the LFP temporal dynamics during SWO, before we discuss the implications of our findings presented in the paper.

We will assume that for the data we have analysed, diffusion currents have negligible effect on the current sink/source estimation. Diffusion currents have been shown to bias CSD analysis of SWOs with frequencies < 1 Hz (Gratny et al., 2017). Our SWO data have an average frequency of around 2 Hz, and the maximum duration of the Up or DD states we used was < 250 ms. Finally, we note that the potential influence of our choice of animal model and anaesthetic regime (rats under ISO) warrant future comparative studies, cf. the section 'Initiation of the Up state was faster from DD than from SD states'.

Effect of voltage-dependent channels on the temporal profile of LFP during SWO

Although the impact of synaptic channel dynamics on the temporal profile of evoked and spontaneous extracellular field potentials has been investigated extensively, many ambiguities are yet to be resolved (Herreras, 2016). In this section, we discuss the extent to which voltage-gated

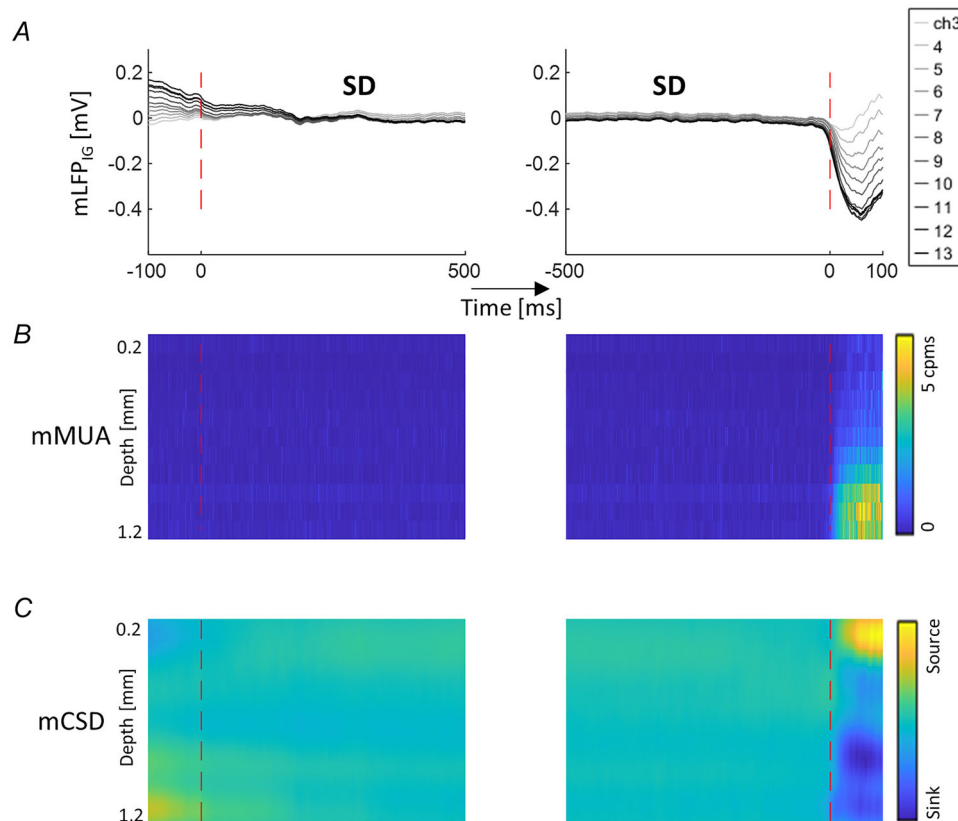


Figure 10. LFP deflections preceding and following sustained SD state

A, mean LFP_G 100 ms preceding sustained SD (left, $n = 224$), and following sustained SD (right, $n = 237$). B, the corresponding MUA. C, the corresponding CSD. A red dashed line marks the time of alignment throughout.

channels may shape the temporal profile of the LFP during spontaneous SWOs.

First, voltage-gated sodium (Na^+) and calcium (Ca^{2+}) channels have been shown to be approximately uniformly distributed along the apical dendrite (Gurkiewicz & Korngreen, 2007; Oakley et al., 2001; Stuart & Sakmann, 1994), and thus these channels are unlikely to induce sources and sinks during SWO even though they may participate in the Up state initiation and termination processes.

An important class of voltage-gated channels implicated in the Up/Down state transition is the voltage-gated potassium (K^+) channels. These include the fast and slow inactivating K^+ channels, as well as inwardly rectifying K^+ channels.

The spatial distribution of inactivating K^+ channels in neocortical pyramidal neurons has been shown to decrease slightly along the apical dendrite (Bekkers, 2000a). These channels are activated during membrane potential V_m depolarisation, passing outward K^+ currents. Thus, they play an important role in controlling spike frequency and Up state duration (Compte et al., 2003b; Contreras et al., 1996). During activation (i.e. Up state), the fast component of the inactivating current typically reaches its peak within 10 ms before decaying to its baseline, while the slow component tends to reach its peak within 20 ms and subsequently decays slowly to a steady state, reducing the excitability of neurons (Bekkers, 2000a, 2000b; Korngreen & Sakmann, 2000; Schaefer et al., 2003). Thus, inactivating K^+ currents during the Up state act in the opposite direction to EPSCs, reducing the strength of the current sinks and sources extracellularly. However, during deactivation when V_m is hyperpolarised, these inactivating currents typically return to baseline within milliseconds (Bekkers, 2000a, 2000b; Korngreen & Sakmann, 2000; Schaefer et al., 2003). Thus, their impact on the prolonged LFP deflection during the DD state is likely to be minimal.

Out of the seven subfamilies of inwardly rectifying K^+ (Kir) channels, the classical Kir and the G protein-activated Kir channels are considered to be involved in the excitability of cortical pyramidal neurons (Compte et al., 2003b; Hibino et al., 2010). Kir channels are activated by hyperpolarisation, with an equilibrium potential for K^+ (-90 mV) below which inward K^+ currents are observed (Hill, 2008; Lu, 2004). They are deactivated during depolarisation. Under physiological conditions when V_m is between the resting potential and the firing potential of neurons (typically between -40 and -80 mV), a small outward K^+ current flows through these channels, effectively lowering the resting membrane potential and decreasing the excitability of neurons (Hill, 2008). This implies that the Kir current is persistent during the resting state. However, no obvious sinks/sources were observed during the SD state in our

data, possibly because these currents are too small to generate measurable sinks and sources at the resting membrane potential. The kinetics of Kir currents were much faster than the duration of the DD state we typically observed (Edwards et al., 1988; Guo et al., 2003; Lu, 2004; Lu et al., 2007), suggesting that the Kir current is unlikely to be the primary source of the depth-positive LFP during the DD state.

In contrast to the classical Kir currents, G protein-activated Kir (GIRK) channels are activated during depolarisation by G protein-coupled receptors (GPCRs) via γ -aminobutyric acid (GABA) neurotransmitters, namely the GABA_B receptors. These GABA_B -mediated GIRK channels have an onset time (about 10 ms, Sanders et al., 2013) dependent on the time required for the diffusion of GABA released into the synaptic cleft (Lüscher & Slesinger, 2010). Furthermore, their decay time constant in the absence of afferent input (i.e. Down state) is of the order 100 ms or longer (Destexhe et al., 1994; Gerstner et al., 2014; Sanders et al., 2013). The density of the GABA_B receptor-mediated GIRK current is higher near the soma where most inhibitory synapses are located (Trevelyan & Watkinson, 2005). Thus, these channels have the potential to generate extracellular current sinks and sources and shape the LFP temporal profile during the Down state. In the discussion below, we will refer to the GABA_B receptor-mediated GIRK current as the IPSC mediated by GABA_B receptors, or simply as the slow IPSC.

Alternating dominance of EPSCs and IPSCs explains LFP deflections during SWOs

We have shown that the sequence of the Up, DD and SD states is not random. Our analysis revealed that the most frequently observed sequences were Up \rightarrow DD \rightarrow SD \rightarrow Up or Up \rightarrow DD \rightarrow Up. The corresponding CSD maps showed sink/source characteristics with opposite polarity during the Up and DD state but not in the SD state. This implies that the net transmembrane current generated a dominant dipole during the Up state. When transitioning to the Down state the net current appeared to have reversed its direction at the initial stage of the Down state, and continued to flow through the extracellular space for much longer than the time taken for the membrane potential to return to its baseline (Timofeev et al., 2012). This transmembrane current weakens over the duration of the Down state, eventually decaying to baseline unless the network becomes active again. However, we argued above that most voltage-gated channels are unable to generate current sources and sinks at this time scale.

An alternative explanation is that the Up, DD and SD states correspond to the activation, deactivation and inactivation, respectively, of both excitatory and inhibitory synaptic channels. Given that synaptic

excitation and inhibition have nearly synchronised onset and cessation (Okun & Lampl, 2008; Shu et al., 2003), we ask: how does this co-tuning phenomenon yield the current sources and sinks, and does it underlie the depth-negative and depth-positive deflections of the LFP and the associated CSD and MUA characteristics? Based on the literature that the IG layer pyramidal neurons play a key role in the spontaneous SWO (McCormick et al., 2003; Neske, 2016; Steriade & Amzica, 1996) and our results presented here, we hypothesise that the dominance of excitation and inhibition in the IG pyramidal neurons is switched between the Up and the Down state such that during the Up state (or activation), EPSC > IPSC, yielding a negative deflection in the LFP_{IG}, a sustained spiking activity or MUA, and an associated sink-source configuration in the IG-SG layer. Conversely during the DD state (or deactivation), IPSC > EPSC, resulting in a positive deflection in the LFP_{IG}, a corresponding source-sink configuration in the IG-SG layer and the cessation of the MUA. The deactivation process moves to inactivation or baseline during prolonged Down states, resulting in the SD state. Once synaptic channels are activated (Up), they cannot transition to inactivation (SD) without going through the process of deactivation (DD). Also synapses in the inactivation state (SD) cannot transition directly to deactivation (DD). This is why the two transitions Up → SD and SD → DD were so unlikely in our data. This also explains our finding that after a sustained period of quiescence, the onset of the LFP activity was marked by a depth-negative deflection, whereas the temporal profile of the LFP leading to a quiescent state was marked by the depth-positive deflection (Fig. 10).

Evidence supporting the alternating dominance of excitation and inhibition can be found from research at the cellular level.

(i) Inhibition has been shown to lag excitation during spontaneous activity of neurons (Berg et al., 2007; Okun & Lampl, 2008; Shu et al., 2003), suggesting that the onset of excitation is earlier and therefore dominates inhibition during the earlier phase of the Up state. Furthermore the GABA_B receptor-mediated inhibitory current has the slowest temporal dynamics compared with other postsynaptic currents, with a deactivation time constant typically >100 ms (Bettler et al., 2004; Destexhe et al., 1994; Gerstner et al., 2014; Lacaille, 1991), and thus is likely to dominate excitation during the latter phase of the deactivation process. We are unable to identify the precise timing of the switch from excitation dominance to inhibition dominance from our data, but several papers on estimating evoked excitatory and inhibitory conductances, G_e and G_i respectively, showed that G_i overtook G_e during the rising phase of the evoked activity (Heiss et al., 2008; Higley & Contreras, 2006; Wilent & Contreras, 2005).

(ii) We suggest that synaptic current components do not reverse their direction of flow individually during SWO, rather the net current influx appears to have switched signs at the IG layer. Evidence for EPSC and IPSC maintaining their direction of flow during SWO can be found in studies using whole-cell patch clamp techniques (Haider et al., 2006; Shu et al., 2003). When the membrane voltage of a cell was clamped at the reversal potential of excitation, a positive current must be injected intracellularly to maintain the membrane potential above its resting potential. During the Up state, there was no influx of EPSC because of the voltage clamping, and only IPSC could be observed. To maintain the clamped voltage, more positive currents must be injected to counter-balance the IPSC. Thus, for this configuration, the Up state was associated with an increase in the injected current. When the Up state transitioned to the Down state, this positive current simply returned to its pre-Up state level without decreasing below the baseline. This time course suggested that IPSC did not reverse its direction of flow. A similar case could be made for the direction of flow of EPSC when the membrane potential was clamped at the reversal potential for inhibition. Thus, both EPSC and IPSC maintained their direction of flow during activation and deactivation. The depth-positive LFP observed in the DD state was therefore primarily generated by the IPSC-dominated current in the IG layer of the neocortex.

Based on the LFP data presented in this paper, we are unable to provide direct evidence for an excitation/inhibition switch during SWO, nor could we calculate the timing of such a switch. Experiments that can provide such insight would be concurrent LFP and whole-cell voltage-clamp recording studies (Haider et al., 2016). As the GABA_B receptor-mediated inhibitory current is a potential key player underlying spontaneous Up and Down states, any GABA_B receptor antagonist, such as QX-314, should be avoided in such studies (Haider et al., 2006; Shu et al., 2003; Wehr & Zador, 2003).

Synaptic mechanisms of Up state initiation

In classifying the two different Down states, we noted that on average the transition SD → Up was significantly slower than DD → Up, as reflected in differences in mLFP_{IG} slopes (Fig. 4A) and MUA onsets and slopes (Fig. 4B). Statistical analysis confirmed that the slopes of transition from DD → Up were consistently faster than SD → Up ones. Examining representative LFP profiles (Fig. 7B and C) suggested that when synaptic activities were at their baseline (SD state), there was a likelihood that mEPSPs temporarily summate in IG layer pyramidal neurons, resulting in their depolarisation and spiking (Chauvette et al., 2010; Neske, 2016).

To examine this hypothesis, we conducted an SUA analysis to examine the onset of APs under the two

transitions. We identified 23 cells and found that, during the DD \rightarrow Up transition, the mean AP onset occurred at the initial phase of the depth-negative LFP_{IG} deflection, whereas during the SD \rightarrow Up transition, the mean AP onset occurred much later when LFP_{IG} reached 60.3% of its negative deflection (Fig. 8D). The LFP and neural spiking activity are known to be tightly locked during a range of brain rhythmic activities, including SWOs (Destexhe et al., 1999; Kohn et al., 2009; Okun et al., 2010). Here this coupling appeared to be different depending on whether the Down state was DD or SD. We further showed that the MUA onset during the SD \rightarrow Up transition was significantly delayed compared to the DD \rightarrow Up transition. These findings provided support for the hypothesis that the Up state initiation from the SD state was driven by AP-independent mEPSP from spontaneous local release of glutamate (Fatt & Katz, 1952; Prange & Murphy, 1999; Ramirez & Kavalali, 2011), and thus spiking was absent during the initial deflection of the LFP.

On the other hand, when synaptic activities were still in the process of deactivation (DD state), inhibition dominated excitation, thus reducing the likelihood of mEPSPs. As a result, more Up states were triggered directly by APs generated by distant or local neurons already in the Up state. The speed of depolarisation was then likely to reflect the dynamics of the AMPA receptors, as their fast kinetics also implied that they returned to baseline quicker during deactivation and were more likely to react to subsequent afferents than other slower synaptic channels which may still be deactivated. Thus, the fast but brief IG layer sink observed in the CSD during the DD \rightarrow Up transition (Fig. 6E, middle panel, red arrow) may be generated by the activation of AMPA channels in response to the onset of recurrent spiking activity. Our data further showed that, on average, the slope of mLFP_{IG} when transitioning to the Up state was invariant to the duration of the preceding DD or SD state, for durations ranging between 100 and 250 ms (Fig. 6E, left). This finding stands against the expectation that longer DD may lead to decreased slope of the LFP deflection because the DD state transitions to SD eventually. One possible explanation is that within the range used in our analysis, the DD may still be dominated by inhibition. If the duration of the DD state is extended beyond 250 ms, it is possible that the average slope for the Up state transition may start to decrease, increasing the likelihood of mEPSP occurrence. However, our data lacked a sufficient number of prolonged DD states beyond 250 ms to yield robust findings.

Synaptic mechanisms of Up state termination

Several possible synaptic and intrinsic mechanisms have been suggested to be involved in Up state termination, including the withdrawal of recurrent spiking activity in the cortical network (Contreras et al., 1996), voltage-gated

inactivating potassium current (Chen et al., 2012; Hill & Tononi, 2005), firing rate adaptation (Sanchez-Vives et al., 2010) and active spiking of a small group of inhibitory neurons towards the end of the Up state to silence targeted excitatory neurons (Chen et al., 2012; Funk et al., 2017; Zucca et al., 2017), sequentially deactivating the cortex (Luczak et al., 2007).

The findings in this paper raise the possibility that during a persistent Up state, the instantaneous balance of excitation and inhibition could shift towards inhibition. This gradual increase of inhibition dominance, together with voltage-gated inactivating K⁺ currents, may act to actively terminate the Up state through hyperpolarising V_m . This is in agreement with several studies that demonstrate the important role GABA_B-mediated IPSCs played in the termination of the Up state (Barbero-Castillo et al., 2021; Craig & McBain, 2014; Mann et al., 2009; Perez-Zabalza et al., 2020). Blocking slow inhibition mediated by GABA_B receptors was shown to significantly extend the duration of the Up state.

We observed that the slope of transition Up \rightarrow DD was independent of the Up state duration within the range 100–175 ms (Fig. 9B). This suggests a scenario with negative feedback leading to a largely stereotyped cessation of neural activity once some threshold has been crossed. We note that particularly long-lasting Up states might be those that narrowly avoid crossing this balance threshold for a variety of reasons. Our (150, 175] ms selection (dark blue in Fig. 9D) suggestively develops like the (100, 125] ms selection (blue in Fig. 9D) until it gets 'bent down' intermittently – perhaps by an unusual burst of incoming excitation – and has to recover to eventually follow the same progression again. However, further experiments are required to determine whether this speculation holds true, and if so, which of the mentioned mechanisms contribute.

Conclusion

We have studied the temporal profile of the LFP during spontaneous Up and Down states and established a novel experimental distinction within the Down state between a dynamic (DD) and a static (SD) phase. By investigating the temporal sequence of occurrence of the Up, DD and SD states, we suggest that these states correspond to the activation, deactivation and inactivation of both excitatory and inhibitory synaptic channels, with a continuous shift of the instantaneous balance between them from excitation dominance (Up) to inhibition dominance (DD). This explains why the sink–source configuration in the CSD map during the DD state has the opposite polarity from that during the Up state.

We have also speculated on the possible synaptic mechanisms associated with Up state initiation and termination based on the SUA analysis as well as on

published data, particularly using whole-cell patch clamping techniques. We suggest that, during SD states, Up states are more likely to be initiated by AP-independent mEPSPs; whereas during DD states, Up states are likely to be triggered by afferent spiking activity. Furthermore, the shift of dominance from excitation to inhibition could be a synaptic mechanism of Up state termination, working in collaboration with other factors. However, based on current data it is not possible to determine if this shift occurs before or after the withdrawal of recurrent activity. It remains an open question whether similar synaptic mechanisms underlie the generation of other brain rhythms, and if so, how the various frequencies of these oscillations come about.

References

- Atallah, B. V., & Scanziani, M., (2009). Instantaneous modulation of gamma oscillation frequency by balancing excitation with inhibition. *Neuron*, **62**(4), 566–577.
- Barbero-Castillo, A., Mateos-Aparicio, P., Dalla Porta, L., Camassa, A., Perez-Mendez, L., & Sanchez-Vives, M. V., (2021). Impact of GABA_B and GABA_A inhibition on cortical dynamics and perturbational complexity during synchronous and desynchronized states. *The Journal of Neuroscience*, **41**(23), 5029–5044.
- Bekkers, J. M., (2000a). Distribution and activation of voltage-gated potassium channels in cell-attached and outside-out patches from large layer 5 cortical pyramidal neurons of the rat. *The Journal of Physiology*, **525**(3), 611–620.
- Bekkers, J. M., (2000b). Properties of voltage-gated potassium currents in nucleated patches from large layer 5 cortical pyramidal neurons of the rat. *The Journal of Physiology*, **525**(3), 593–609.
- Berg, R. W., Alaburda, A., & Hounsgaard, J., (2007). Balanced Inhibition and excitation drive spike activity in spinal half-centers. *Science*, **315**(5810), 390–393.
- Berg, R. W., & Ditlevsen, S., (2013). Synaptic inhibition and excitation estimated via the time constant of membrane potential fluctuations. *Journal of Neurophysiology*, **110**(4), 1021–1034.
- Bettler, B., Kaupmann, K., Mosbacher, J., & Gassmann, M., (2004). Molecular structure and physiological functions of GABA(B) receptors. *Physiological Reviews*, **84**(3), 835–867.
- Buzsáki, G., Anastassiou, C. A., & Koch, C., (2012). The origin of extracellular fields and currents — EEG, ECoG, LFP and spikes. *Nature Reviews Neuroscience*, **13**(6), 407–420.
- Castro-Alamancos, M. A., (2004). Dynamics of sensory thalamocortical synaptic networks during information processing states. *Progress in Neurobiology*, **74**(4), 213–247.
- Chauvette, S., Volgushev, M., & Timofeev, I., (2010). Origin of active states in local neocortical networks during slow sleep oscillation. *Cerebral Cortex*, **20**(11), 2660–2674.
- Chen, J.-Y., Chauvette, S., Skorheim, S., Timofeev, I., & Bazhenov, M., (2012). Interneuron-mediated inhibition synchronizes neuronal activity during slow oscillation. *The Journal of Physiology*, **590**(16), 3987–4010.
- Compte, A., Sanchez-Vives, M. V., McCormick, D. A., & Wang, X.-J., (2003a). Cellular and network mechanisms of slow oscillatory activity (<1 Hz) and wave propagations in a cortical network model. *Journal of Neurophysiology*, **89**, 2707–2725.
- Compte, A., Sanchez-Vives, M. V., McCormick, D. A., & Wang, X. J., (2003b). Cellular and network mechanisms of slow oscillatory activity (<1 Hz) and wave propagations in a cortical network model. *Journal of Neurophysiology*, **89**, 2707–2725.
- Constantinople, C. M., & Bruno, R. M., (2013). Deep cortical layers are activated directly by thalamus. *Science*, **340**(6140), 1591–1594.
- Contreras, D., & Steriade, M., (1995). Cellular basis of EEG slow rhythms: A study of dynamic corticothalamic relationships. *The Journal of Neuroscience*, **15**(1), 604–622.
- Contreras, D., Timofeev, I., & Steriade, M., (1996). Mechanisms of long-lasting hyperpolarizations underlying slow sleep oscillations in cat corticothalamic networks. *The Journal of Physiology*, **494**(Pt 1), 251–264.
- Craig, M. T., & Mcbain, C. J., (2014). The emerging role of GABA_B receptors as regulators of network dynamics: Fast actions from a ‘slow’ receptor? *Current Opinion in Neurobiology*, **26**, 15–21.
- Csicsvari, J., Hirase, H., Czurko, A., & Buzsáki, G., (1998). Reliability and state dependence of pyramidal cell-interneuron synapses in the hippocampus: An ensemble approach in the behaving rat. *Neuron*, **21**(1), 179–189.
- Csicsvari, J., Hirase, H., Czurkó, A., Mamiya, A., & Buzsáki, G., (1999). Oscillatory coupling of hippocampal pyramidal cells and interneurons in the behaving rat. *The Journal of Neuroscience*, **19**(1), 274–287.
- Destexhe, A., Contreras, D., & Steriade, M., (1999). Spatiotemporal analysis of local field potentials and unit discharges in cat cerebral cortex during natural wake and sleep states. *Journal of Neuroscience*, **19**(11), 4595–4608.
- Destexhe, A., Hughes, S. W., Rudolph, M., & Crunelli, V., (2007). Are corticothalamic ‘up’ states fragments of wakefulness? *Trends in Neurosciences*, **30**(7), 334–342.
- Destexhe, A., Mainen, Z. F., & Sejnowski, T. J., (1994). Synthesis of models for excitable membranes, synaptic transmission and neuromodulation using a common kinetic formalism. *Journal of Computational Neuroscience*, **1**(3), 195–230.
- Devonshire, I. M., Mayhew, J. E. W., & Overton, P. G., (2007). Cocaine preferentially enhances sensory processing in the upper layers of the primary sensory cortex. *Neuroscience*, **146**(2), 841–851.
- Edwards, F. R., Hirst, G. D., & Silverberg, G. D., (1988). Inward rectification in rat cerebral arterioles; involvement of potassium ions in autoregulation. *The Journal of Physiology*, **404**(1), 455–466.
- Einevoll, G. T., Kayser, C., Logothetis, N. K., & Panzeri, S., (2013). Modelling and analysis of local field potentials for studying the function of cortical circuits. *Nature Reviews Neuroscience*, **14**(11), 770–785.
- Fatt, P., & Katz, B., (1952). Spontaneous subthreshold activity at motor nerve endings. *The Journal of Physiology*, **117**(1), 109–128.

- Fiáth, R., Kerekes, B. P., Wittner, L., Tóth, K., Beregszászi, P., Horváth, D., & Ulbert, I., (2016). Laminar analysis of the slow wave activity in the somatosensory cortex of anesthetized rats. *European Journal of Neuroscience*, **44**(3), 1935–1951.
- Friedberg, M. H., Lee, S. M., & Ebner, F. F., (1999). Modulation of receptive field properties of thalamic somatosensory neurons by the depth of anesthesia. *Journal of Neurophysiology*, **81**(5), 2243–2252.
- Funk, C. M., Peelman, K., Bellesi, M., Marshall, W., Cirelli, C., & Tononi, G., (2017). Role of somatostatin-positive cortical interneurons in the generation of sleep slow waves. *Journal of Neuroscience*, **37**(38), 9132–9148.
- Gerstner, W., Kistler, W. M., Naud, R., & Paninski, L., (2014). *Neuronal Dynamics: From Single Neurons to Networks and Models of Cognition*. Cambridge University Press, Cambridge.
- Gratiy, S. L., Halnes, G., Denman, D., Hawrylycz, M. J., Koch, C., Einevoll, G. T., & Anastassiou, C. A., (2017). From Maxwell's equations to the theory of current-source density analysis. *European Journal of Neuroscience*, **45**(8), 1013–1023.
- Grundy, D., (2015). Principles and standards for reporting animal experiments in The Journal of Physiology and Experimental Physiology. *The Journal of Physiology*, **593**(12), 2547–2549.
- Guo, D., Ramu, Y., Klem, A. M., & Lu, Z., (2003). Mechanism of rectification in inward-rectifier K⁺ channels. *Journal of General Physiology*, **121**(4), 261–276.
- Gurkiewicz, M., & Korngreen, A., (2007). Recording, analysis, and function of dendritic voltage-gated channels. *Pflügers Archiv: European journal of physiology*, **453**(3), 283–292.
- Haider, B., Duque, A., Hasenstaub, A. R., & McCormick, D. A., (2006). Neocortical network activity in vivo is generated through a dynamic balance of excitation and inhibition. *Journal of Neuroscience*, **26**(17), 4535–4545.
- Haider, B., & McCormick, D. A., (2009). Rapid neocortical dynamics: Cellular and network mechanisms. *Neuron*, **62**(2), 171–189.
- Haider, B., Schulz, D. P. A., Häusser, M., & Carandini, M., (2016). Millisecond coupling of local field potentials to synaptic currents in the awake visual cortex. *Neuron*, **90**(1), 35–42.
- Harris, K. D., Hirase, H., Leinekugel, X., Henze, D. A., & Buzsáki, G., (2001). Temporal interaction between single spikes and complex spike bursts in hippocampal pyramidal cells. *Neuron*, **32**(1), 141–149.
- Heiss, J. E., Katz, Y., Ganmor, E., & Lampl, I., (2008). Shift in the balance between excitation and inhibition during sensory adaptation of S1 neurons. *Journal of Neuroscience*, **28**(49), 13320–13330.
- Herreras, O., (2016). Local field potentials: Myths and misunderstandings. *Frontiers in Neural Circuits*, **10**, 101.
- Hibino, H., Inanobe, A., Furutani, K., Murakami, S., Findlay, I., & Kurachi, Y., (2010). Inwardly rectifying potassium channels: Their structure, function, and physiological roles. *Physiological Reviews*, **90**(1), 291–366.
- Higley, M. J., & Contreras, D., (2006). Balanced excitation and inhibition determine spike timing during frequency adaptation. *The Journal of Neuroscience*, **26**(2), 448–457.
- Hill, C. E., (2008). Inward rectification and vascular function: As it was in the beginning. *The Journal of Physiology*, **586**(6), 1465–1467.
- Hill, S., & Tononi, G., (2005). Modeling sleep and wakefulness in the thalamocortical system. *Journal of Neurophysiology*, **93**(3), 1671–1698.
- Huck, S. W., (2008). *Reading Statistics and Research*. Pearson/Allyn & Bacon.
- Kang, S., Bruyins-Haylett, M., Hayashi, Y., & Zheng, Y., (2017). Concurrent recording of co-localized electroencephalography and local field potential in rodent. *Journal of Visualized Experiments: JoVE*, e56447.
- Kang, S., Hayashi, Y., Bruyins-Haylett, M., Delivopoulos, E., & Zheng, Y., (2020). Model-predicted balance between neural excitation and inhibition was maintained despite of Age-related decline in sensory evoked local field potential in rat barrel cortex. *Frontiers in Systems Neuroscience*, **14**, 24–24.
- Kohn, A., Zandvakili, A., & Smith, M. A., (2009). Correlations and brain states: From electrophysiology to functional imaging. *Current Opinion in Neurobiology*, **19**(4), 434–438.
- Korngreen, A., & Sakmann, B., (2000). Voltage-gated K⁺ channels in layer 5 neocortical pyramidal neurones from young rats: Subtypes and gradients. *The Journal of Physiology*, **525**(Pt 3), 621–639.
- Kroeger, D., & Amzica, F., (2007). Hypersensitivity of the anesthesia-induced comatose brain. *Journal of Neuroscience*, **27**(39), 10597–10607.
- Lacaille, J. C., (1991). Postsynaptic potentials mediated by excitatory and inhibitory amino acids in interneurons of stratum pyramidale of the CA1 region of rat hippocampal slices in vitro. *Journal of Neurophysiology*, **66**(5), 1441–1454.
- Logothetis, N. K., (2003). The Underpinnings of the BOLD functional magnetic resonance imaging signal. *Journal of Neuroscience*, **23**(10), 3963–3971.
- Lu, B., Su, Y., Das, S., Liu, J., Xia, J., & Ren, D., (2007). The neuronal channel NALCN contributes resting sodium permeability and is required for normal respiratory rhythm. *Cell*, **129**(2), 371–383.
- Lu, Z., (2004). Mechanism of rectification in inward-rectifier K⁺ channels. *Annual Review of Physiology*, **66**(1), 103–129.
- Luczak, A., Barthó, P., Marguet, S. L., Buzsáki, G., & Harris, K. D., (2007). Sequential structure of neocortical spontaneous activity in vivo. *Proceedings of the National Academy of Sciences, USA*, **104**(1), 347–352.
- Lüscher, C., & Slesinger, P. A., (2010). Emerging roles for G protein-gated inwardly rectifying potassium (GIRK) channels in health and disease. *Nature Reviews Neuroscience*, **11**(5), 301–315.
- Mann, E. O., Kohl, M. M., & Paulsen, O., (2009). Distinct roles of GABAA and GABAB receptors in balancing and terminating persistent cortical activity. *The Journal of Neuroscience*, **29**(23), 7513–7518.
- Martin, C., Zheng, Y., Sibson, N. R., Mayhew, J. E. W., & Berwick, J., (2013). Complex spatiotemporal haemodynamic response following sensory stimulation in the awake rat. *Neuroimage*, **66**, 1–8.
- McCormick, D. A., Mcginley, M. J., & Salkoff, D. B., (2015). Brain state dependent activity in the cortex and thalamus. *Current Opinion in Neurobiology*, **31**, 133–140.

- Mccormick, D. A., & Pape, H. C., (1990). Properties of a hyperpolarization-activated cation current and its role in rhythmic oscillation in thalamic relay neurones. *The Journal of Physiology*, **431**(1), 291–318.
- Mccormick, D. A., (2003). Persistent cortical activity: Mechanisms of generation and effects on neuronal excitability. *Cerebral Cortex*, **13**(11), 1219–1231.
- Mitzdorf, U., (1985). Current source-density method and application in cat cerebral cortex: Investigation of evoked potentials and EEG phenomena. *Physiological Reviews*, **65**(1), 37–100.
- Mizuseki, K., Diba, K., Pastalkova, E., & Buzsáki, G., (2011). Hippocampal CA1 pyramidal cells form functionally distinct sublayers. *Nature Neuroscience*, **14**(9), 1174–1181.
- Narayanan, R. T., Udvary, D., & Oberlaender, M., (2017). Cell type-specific structural organization of the six layers in rat barrel cortex. *Frontiers in Neuroanatomy*, **11**, 91.
- Neske, G. T., (2016). The slow oscillation in cortical and thalamic networks: Mechanisms and functions. *Frontiers in Neural Circuits*, **9**, 88.
- Neske, G. T., Patrick, S. L., & Connors, B. W., (2015). Contributions of diverse excitatory and inhibitory neurons to recurrent network activity in cerebral cortex. *The Journal of Neuroscience*, **35**(3), 1089–1105.
- O'Neill, J., Boccarda, C. N., Stella, F., Schoenenberger, P., & Csicsvari, J., (2017). Superficial layers of the medial entorhinal cortex replay independently of the hippocampus. *Science*, **355**(6321), 184–188.
- Oakley, J. C., Schwandt, P. C., & Crill, W. E., (2001). Initiation and propagation of regenerative Ca^{2+} -dependent potentials in dendrites of layer 5 pyramidal neurons. *Journal of Neurophysiology*, **86**(1), 503–513.
- Oberlaender, M., De Kock, C. P. J., Bruno, R. M., Ramirez, A., Meyer, H. S., Derksen, V. J., Helmstaedter, M., & Sakmann, B., (2011). Cell type-specific three-dimensional structure of thalamocortical circuits in a column of rat vibrissal cortex. *Cerebral Cortex*, **22**(10), 2375–2391.
- Okun, M., & Lampl, I., (2008). Instantaneous correlation of excitation and inhibition during ongoing and sensory-evoked activities. *Nature Neuroscience*, **11**(5), 535–537.
- Okun, M., Naim, A., & Lampl, I., (2010). The subthreshold relation between cortical local field potential and neuronal firing unveiled by intracellular recordings in awake rats. *Journal of Neuroscience*, **30**(12), 4440–4448.
- Paxinos, G., & Watson, C., (2005). *The Rat Brain in Stereotaxic Coordinates*. Elsevier Academic Press.
- Perez-Zabalza, M., Reig, R., Manrique, J., Jercog, D., Winograd, M., Parga, N., & Sanchez-Vives, M. V., (2020). Modulation of cortical slow oscillatory rhythm by GABA_B receptors: An in vitro experimental and computational study. *The Journal of Physiology*, **598**(16), 3439–3457.
- Petersen, C. C. H., (2007). The functional organization of the barrel cortex. *Neuron*, **56**(2), 339–355.
- Petersen, P. C., Vestergaard, M., Jensen, K. H. R., & Berg, R. W., (2014). Premotor spinal network with balanced excitation and inhibition during motor patterns has high resilience to structural division. *The Journal of Neuroscience*, **34**(8), 2774–2784.
- Pettersen, K. H., Devor, A., Ulbert, I., Dale, A. M., & Einevoll, G. T., (2006). Current-source density estimation based on inversion of electrostatic forward solution: Effects of finite extent of neuronal activity and conductivity discontinuities. *Journal of Neuroscience Methods*, **154**(1–2), 116–133.
- Pettersen, K. H., Hagen, E., & Einevoll, G. T., (2008). Estimation of population firing rates and current source densities from laminar electrode recordings. *Journal of Computational Neuroscience*, **24**(3), 291–313.
- Prange, O., & Murphy, T. H., (1999). Correlation of miniature synaptic activity and evoked release probability in cultures of cortical neurons. *The Journal of Neuroscience*, **19**(15), 6427–6438.
- Quiroga, R. Q., Nadasdy, Z., & Ben-Shaul, Y., (2004). Unsupervised spike detection and sorting with wavelets and superparamagnetic clustering. *Neural Computation*, **16**(8), 1661–1687.
- Ramirez, D. M.o., & Kavalali, E. T., (2011). Differential regulation of spontaneous and evoked neurotransmitter release at central synapses. *Current Opinion in Neurobiology*, **21**(2), 275–282.
- Rudolph, M., Pospischil, M., Timofeev, I., & Destexhe, A., (2007). Inhibition determines membrane potential dynamics and controls action potential generation in awake and sleeping cat cortex. *Journal of Neuroscience*, **27**(20), 5280–5290.
- Saleem, A. B., Chadderton, P., Apergis-Schoute, J., Harris, K. D., & Schultz, S. R., (2010). Methods for predicting cortical UP and DOWN states from the phase of deep layer local field potentials. *Journal of Computational Neuroscience*, **29**(1–2), 49–62.
- Sanchez-Vives, M. V., Mattia, M., Compte, A., Perez-Zabalza, M., Winograd, M., Descalzo, V. F., & Reig, R., (2010). Inhibitory modulation of cortical up states. *Journal of Neurophysiology*, **104**(3), 1314–1324.
- Sanchez-Vives, M. V., & Mccormick, D. A., (2000). Cellular and network mechanisms of rhythmic recurrent activity in neocortex. *Nature Neuroscience*, **3**(10), 1027–1034.
- Sanders, H., Berends, M., Major, G., Goldman, M. S., & Lisman, J. E., (2013). NMDA and GABA_B (KIR) Conductances: The “Perfect Couple” for Bistability. *The Journal of Neuroscience*, **33**(2), 424–429.
- Schaefer, A. T., Helmstaedter, M., Sakmann, B., & Korngreen, A., (2003). Correction of conductance measurements in non-space-clamped structures: I. Voltage-gated K^{+} channels. *Biophysical Journal*, **84**(6), 3508–3528.
- Schwandt, P. C., Spain, W. J., & Crill, W. E., (1992). Calcium-dependent potassium currents in neurons from cat sensorimotor cortex. *Journal of Neurophysiology*, **67**(1), 216–226.
- Shu, Y., Hasenstaub, A., & Mccormick, D. A., (2003). Turning on and off recurrent balanced cortical activity. *Nature*, **423**(6937), 288–293.
- Steriade, M., & Amzica, F., (1996). Intracortical and cortico-thalamic coherency of fast spontaneous oscillations. *Proceedings of the National Academy of Sciences, USA*, **93**(6), 2533–2538.

- Steriade, M., Nunez, A., & Amzica, F., (1993). A novel slow (<1 Hz) oscillation of neocortical neurons in vivo: Depolarizing and hyperpolarizing components. *The Journal of Neuroscience*, **13**, 3252–3265.
- Stuart, G. J., & Sakmann, B., (1994). Active propagation of somatic action potentials into neocortical pyramidal cell dendrites. *Nature*, **367**(6458), 69–72.
- Timofeev, I., Bazhenov, M., Seigneur, J., & Sejnowski, T., (2012). Neuronal Synchronization and Thalamocortical Rhythms in Sleep, Wake and Epilepsy. In: Noebels, J.L., Avoli, M., Rogawski, M.A., Olsen, R.W., Delgado-Escueta, A.V. (Eds.), *Jasper's Basic Mechanisms of the Epilepsies*. National Center for Biotechnology Information (US). Copyright © 2012, Michael A Rogawski, Antonio V Delgado-Escueta, Jeffrey L Noebels, Massimo Avoli and Richard W Olsen., Bethesda (MD).
- Timofeev, I., Contreras, D., & Steriade, M., (1996). Synaptic responsiveness of cortical and thalamic neurones during various phases of slow sleep oscillation in cat. *The Journal of Physiology*, **494**(1), 265–278.
- Timofeev, I., (2000). Origin of slow cortical oscillations in deafferented cortical slabs. *Cerebral Cortex*, **10**(12), 1185–1199.
- Timofeev, I., Schoch, S. F., Lebourgeois, M. K., Huber, R., Riedner, B. A., & Kurth, S., (2020). Spatio-temporal properties of sleep slow waves and implications for development. *Current Opinion in Physiology*, **15**, 172–182.
- Torao-Angosto, M., Manasanch, A., Mattia, M., & Sanchez-Vives, M. V., (2021). Up and Down states during slow oscillations in slow-wave sleep and different levels of anesthesia. *Frontiers in Systems Neuroscience*, **15**, 609645.
- Trevelyan, A. J., & Watkinson, O., (2005). Does inhibition balance excitation in neocortex? *Progress in Biophysics and Molecular Biology*, **87**(1), 109–143.
- Wehr, M., & Zador, A. M., (2003). Balanced inhibition underlies tuning and sharpens spike timing in auditory cortex. *Nature*, **426**(6965), 442–446.
- Wilent, W. B., & Contreras, D., (2005). Dynamics of excitation and inhibition underlying stimulus selectivity in rat somatosensory cortex. *Nature Neuroscience*, **8**(10), 1364–1370.
- Wuarin, J.p., & Dudek, F.e., (1993). Patch-clamp analysis of spontaneous synaptic currents in supraoptic neuroendocrine cells of the rat hypothalamus. *Journal of Neuroscience*, **13**(6), 2323–2331,
- Ye, H., Jalini, S., Zhang, L., Charlton, M., & Carlen, P. L., (2010). Early ischemia enhances action potential-dependent, spontaneous glutamatergic responses in CA1 neurons. *Journal of Cerebral Blood Flow and Metabolism*, **30**(3), 555–565.
- Zucca, S., D'urso, G., Pasquale, V., Vecchia, D., Pica, G., Bovetti, S., Moretti, C., Varani, S., Molano-Mazón, M., Chiappalone, M., Panzeri, S., & Fellin, T., (2017). An inhibitory gate for state transition in cortex. *eLife*, **6**, e26177.

Additional information

Data availability statement

Data and MATLAB code will be made available by the corresponding author upon request without undue reservation.

Competing interests

None.

Author contributions

Y.Z.: conceptualization; data curation; formal analysis; investigation; resources; methodology; software; supervision; project administration; validation; visualization; writing – original draft; writing – review and editing. S.K.: data curation; investigation; formal analysis; software; validation; writing – review and editing. J.O'N.: formal analysis; methodology; software; validation; writing – review and editing. I.B.: formal analysis; methodology; validation; visualization; writing – review and editing. All authors have read and approved the final version of this manuscript and agree to be accountable for all aspects of the work in ensuring that questions related to the accuracy or integrity of any part of the work are appropriately investigated and resolved. All persons designated as authors qualify for authorship, and all those who qualify for authorship are listed.

Funding

The work was supported by the BBSRC (grant number: BB/K010123/1).

Acknowledgements

The authors would like to thank Andrew Cripps, Mhairi Baxter, and the BioResource Unit at the University of Reading. The authors are indebted to Dr Michael Bruyns-Haylett and Dr Jingjing Luo for some MATLAB programmes that were used in our data pre-processing and analysis.

Keywords

balance of excitation and inhibition, extracellular field potential, slow-wave oscillation, spontaneous, up state initiation, up state termination

Supporting information

Additional supporting information can be found online in the Supporting Information section at the end of the HTML view of the article. Supporting information files available:

Statistical Summary Document
Peer Review History